Contemporary Issues in Electron Transfer Research

Paul F. Barbara*

Department of Chemistry, University of Minnesota, Minneapolis, Minnesota 55455

Thomas J. Meyer*

Department of Chemistry, University of North Carolina, Chapel Hill, North Carolina 27599

Mark A. Ratner*

Department of Chemistry, Northwestern University, Evanston, Illinois 60208

Received: February 23, 1996; In Final Form: April 30, 1996[⊗]

This is an overview of some of the important, challenging, and problematic issues in contemporary electron transfer research. After a qualitative discussion of electron transfer, its time and distance scales, energy curves, and basic parabolic energy models are introduced to define the electron transfer process. Application of transition state theory leads to the standard Marcus formulation of electron transfer rate constants. Electron transfer in solution is coupled to solvent polarization effects, and relaxation processes can contribute to and even control electron transfer. The inverted region, in which electron transfer rate constants decrease with increasing exoergicity, is one of the most striking phenomena in electron transfer chemistry. It is predicted by both semiclassical and quantum mechanical models, with the latter appropriate if there are coupled high- or medium-frequency vibrations. The intramolecular reorganizational energy has different contributions from different vibrational modes, which, in favorable cases, can be measured on a mode-by-mode basis by resonance Raman spectroscopy. Alternatively, mode-averaging procedures are available for including multimode contributions based on absorption or emission spectra. Rate constants for intramolecular electron transfer depend on electronic coupling and orbital overlap and, therefore, on distance. Mixed-valence systems have provided an important experimental platform for investigating solvent and structural effects and the transition between localized and delocalized behavior. One of the important developments in electron transfer is the use of absorption and emission measurements to calculate electron transfer rate constants. Ultrafast electron transfer measurements have been used to uncover nonequilibrium relaxation effects, an area that presents special challenges to the understanding of the dynamics and relaxation of the coupled processes. Electron transfer in the gas phase offers substantial insights into the nature of the electron transfer process. Similarly, electron transport in conductive polymers and synthetic metals depends on the basic principles of electron transfer, with some special nuances of their own.

I. Introduction

A. Qualitative Overview. Electron transfer is one of the prototypical chemical reactions. In first year chemistry books, it is ordinarily classed with neutralization and precipitation reactions as one of the fundamental types. Electron transfer is ubiquitous in biological, physical, inorganic, and organic chemical systems. Understanding and control of electron transfer reactions comprises one of the broadest and most active research areas of physical chemistry today.

Electron transfer (ET) occurs in nature in connection with the transduction of energy. In the photosynthetic reaction center, ET is used to create charge imbalance across a membrane, which eventually drives a proton pumping mechanism to produce ATP. In oxidative phosphorylation, NADH releases electrons to dioxygen, to form water and a substantial amount of excess energy, used to make ATP. Many coupled ET events, such as the four sequential electron transfers from cytochrome to the cytochrome oxidase complex, are crucial to the function of the respiratory chain.

In chemical systems, surface electron transfer between metals and oxygen is responsible for corrosion in electrochemical systems. In organic chemistry, mechanisms involving bond

fracture or bond making (such as the benzyl halide radical formation of eq I.1) very often proceed by an electron transfer mechanism.

$$\text{Na} + \langle\bigcirc\rangle\!-\!\text{CH}_2\!-\!\text{Br} \xrightarrow{\text{DMF}} \text{Na}^+ + \langle\bigcirc\rangle\!-\!\text{CH}_2{}^{\bullet} + \text{Br}^- \quad (\text{I.1})$$
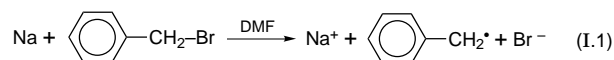
In inorganic chemistry, mixed-valence systems are characterized by electron transfer between linked metal sites. The solid state electronics age depends critically on the control of electron transfer and electron transport in semiconductors. Finally, the nascent area of molecular electronics depends, first and foremost, on understanding and controlling the transfer of electrons in designed chemical structures.

ET causes a change in chemical structure. The simplest way to understand how this impacts electron transfer can be seen in the molecular crystal model in Figure 1. The two schematically indicated diatomics might, for example, be $H_2{}^+$ and H_2. The one-electron cation is less strongly bound and has a longer bond length. If the molecules are rotationally and translationally frozen, only their relative bond distances vary. As the molecules oscillate, they eventually pass through a state in which they are of the same length, following which they may return to the initial configuration (shorter species on the left) or pass to the final

---

Contemporary Issues in Electron Transfer Research

J. Phys. Chem., Vol. 100, No. 31, 1996 **13149**
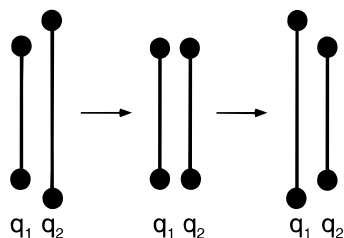
Figure 1. A rudimentary model for an electron transfer reaction involving two diatomic molecules at fixed separation. The two schematically indicated diatomics might, for example, be H_2^+ and H_2.
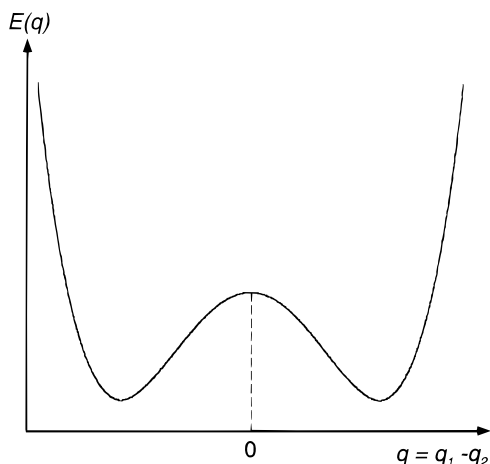
Figure 2. A schematic potential energy diagram for the simple electron transfer example in Figure 1. The two minima correspond to the left and right structures in Figure 1.

state, in which molecule 2 has become shorter—this is because the electron has transferred from molecule 1 to molecule 2. Note that, in this description, the electron itself is not discussed explicitly; the entire process is described in terms of the nuclear geometries of the two diatomics. In order for electron transfer to occur, there must be a perturbation between sites and electronic orbital mixing. Nonetheless, the electron transfer barrier can be understood in a very simple way by the potential energy diagram of Figure 2. The two minima correspond to the left and right structures in Figure 1. The top of the barrier corresponds to the geometry at which the two bond lengths are the same—this is often called the coincidence event geometry. If nuclear tunneling is unimportant, the rate of the ET reaction, from activated complex theory, is simply the rate of crossing the barrier top times its relative population. The latter is the activation energy for electron transfer.

ET reactions are described in terms of the nuclear geometries (molecular structure) of the reactant and the product. The process by which the reactants become products depends on precisely how the barrier is passed over, tunneled through, or otherwise avoided. This is the topic of electron transfer kinetics and rate theory.

The two molecules in Figure 1 could be considered as separate or as bonded together with the same result. In either case, if the relative separations are fixed, the electron transfer barrier depends only upon the lengths q_1 and q_2. Linked systems and intramolecular electron transfer have been the primary focus in recent research, because the relative orientations and geometries of the donor and acceptor sites are fixed by covalent bonding free of diffusional effects. In many systems of primary chemical interest, however, one must worry first about assembling the reactants by diffusional encounter. This can involve overcoming work terms arising largely from electrostatic interaction, and electron transfer is averaged over many possible relative

orientations and geometries. For the remainder of this discussion, we will largely ignore the issues associated with diffusion and assembly of the reactants and assume that ET is intramolecular.

B. Time and Distance Scales for Electron Transfer. Time scales for ET can be as slow as one wishes, because the rate is controlled by the extent of electronic coupling and tunneling either through or crossing over barriers of the type in Figure 2. In the mitochondrial inner membrane, collision-induced electron transfer between the ubiquinone and cytochrome c components occurs roughly every 5−20 ms; leakages across junctions in semiconductor devices are designed to take months, if charge memories are to be stable. Intermolecular electron transfer that depends on diffusion can be essentially infinitely slow in glassy systems where diffusion is completely arrested.

At the other extreme of time, electron transfers following photoexcitation can occur on time scales determined by the electronic mixing between donor and acceptor states. This can actually be faster than the vibrational time required for geometrical changes if electron transfer occurs before vibrational relaxation. Under these conditions simple first-order kinetic rate laws are not necessarily observed. In a number of such fast photoinduced ET reactions, time scales below 100 fs have been measured (section XI).

Experimentally, observation of ultrafast ET is obtained with femtosecond lasers; slower ET can be studied with a variety of techniques such as single photon counting, calorimetric observation, stopped flow mixing, dipole relaxation, or redox titrations. The simple barrier picture of Figure 2 suggests that control of the barrier height is a major factor in controlling time scale. Indeed, achieving such control by a combination of barrier height and the extent of electronic coupling has been the aim of many ET studies.

If ET between a donor D and acceptor A is not enhanced by electronic mixing with the intervening space one expects the rate constant to decrease exponentially with distance consistent with the exponential radial dependence of the electron wave function. Thus, unless electrons are transported either by localization and hopping among intervening sites between D and A or by resonance through the intervening chemical structure, characteristic distances of much greater than 20 Å are not to be expected. Long-range ET has been observed over distances on the order of, say, 27 Å in photosynthetic reaction centers. Very long-range ET occurs by coherent band-type motions (as in metals), by electron hopping (as in disordered semiconductors), or by transport of defect composite particles consisting of an electronic charge and the associated lattice polarization. The latter is the so-called soliton defect that characterizes conduction in a number of conjugated polymers.

The dominant challenge in ET kinetics is gaining a detailed understanding of how the dynamics (rate constants and barriers) for ET reactions are determined by the molecular and electronic structures of the reactants, the nature of the interaction between them, how the initial states are prepared, and the overall energetics.

The general approach in this paper is not to present a systematic overview, but to stress the roles of perspective and intuition and of theory and experiment. We will discuss some of the long-term goals of electron transfer chemistry, questions that remain open and unsolved, and the current level of understanding. Certain historical understandings will be emphasized to provide an appropriate background. The length devoted to a particular topic is not intended as an indication of the current importance of that topic and reflects, in part, the biases of the authors.
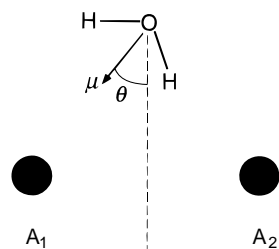
Figure 3. A simple model for the coupling of an electron transfer reaction to a single water (solvent) molecule. There are two electron localization sites, A_1 and A_2. The water molecule, with its oxygen atom fixed in space, is free to rotate and lies above the midpoint between A_1 and A_2.
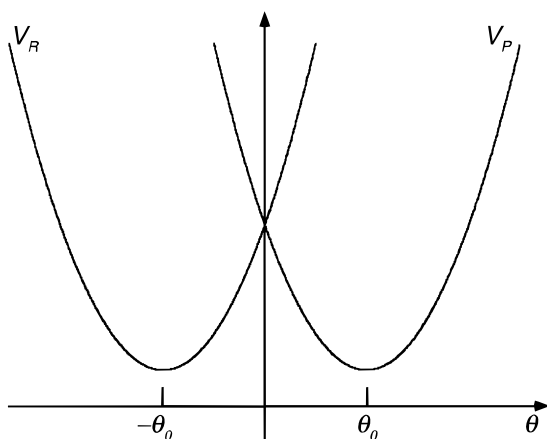
Figure 4. Diabatic potential energy curves for a symmetrical electron transfer reaction, such as that in Figure 3. In this simple situation, the R and P states arise from the excess electron localized at A_1 and A_2, respectively.

II. Potential Curves and Electron Transfer: The Basic Parabola Model

Consider the simple situation illustrated in Figure 3. There are two electron localization sites, A_1 and A_2. (They could, for example, be metal ions.) A water molecule, with its oxygen atom fixed in space, is free to rotate and lies above the midpoint between A_1 and A_2. The dipole moment μ of the water molecule makes an angle θ with a perpendicular bisector of the line between A_1 and A_2. If the electron is localized on A_1, the dipole will tend to point toward A_1; similarly, if the electron is localized on A_2, the dipole will tend to point toward A_2. If the distance between A_1 and A_2 is large enough, there will be two stable positions for the angle θ: one of these will be with the electron on A_1 with $\theta = -\theta_0$. Similarly, with the electron on A_2, the stable position occurs at $\theta = \theta_0$. Around these minima, the total potential curve for rotation of the water molecule approximates a parabola; the two parabolas shown in Figure 4 represent this motion and should be compared with the double-well curve shown in Figure 2. These two situations are essentially identical. In both, changes in nuclear geometry (bond length or orientational angle) cause the electron to be localized in one of the two positions (in Figure 1, on either diatomic; in Figure 3, on either localization site). Note that the two potential curves in Figure 4 are indicated as crossing, whereas in Figure 2 there is only one potential curve, which exhibits a double minimum. In discussing electron transfer, these two representations are generally referred to as diabatic and adiabatic representations, respectively.[1-11]

We can represent the potential energy curves in the convenient diabatic representation of Figure 4. Let us take the generic nuclear coordinate q to represent either the difference in displacements in Figure 2 or the angular displacement in Figure

4. Diabatic curves can then be approximated by the parabolic forms of eqs II.1 and II.2, where f is a force constant. The potential curves for a situation such as in Figures 1 and 3, with symmetric reactant and product ($\Delta G^0 = 0$), are for the reactants, V_R, and products, V_P,

$$V_R = {}^1\!/_2 f(q + q_0)^2 \tag{II.1}$$

$$V_P = {}^1\!/_2 f(q - q_0)^2 \tag{II.2}$$

R and P correspond to the charge distribution before and after the electron transfer; q_0 is the value of q at the minimum. The difference between these two potential energies is given by (II.3), which can be rewritten as (II.4).

$$V_R - V_P = 2fq_0q \tag{II.3}$$

$$q = \frac{1}{2fq_0}(V_R - V_P) \tag{II.4}$$

Equation II.4 is important: it shows that the (physical) distance q, which could be either an angular orientation or a difference between two bond lengths, is linearly related to the difference in potential energies between curves R and P. This includes coupled vibrations treated classically. The most important steps in the formulation of electron transfer rate theory were based on the understanding that for more complicated reactions, such as might occur between large molecules in solution, the coordinates of the problem could number many thousands because of involvement by the solvent. Nevertheless, the potential energies V_R and V_P are uniquely defined for any set of the physical displacements in the system.[11,12] Therefore, just as in our very simple examples of Figures 1 and 3, one could use either q or $(V_R - V_P)$ as the reaction coordinate, since they are linearly related to one another. Because of the involvement of many coordinates in solution, the appropriate reaction coordinate is the difference in potential energies, $V_R - V_P$.[13]

Another generalization is needed. For reactions in solution, it is appropriate to consider not the energy difference, but rather the free energy difference, as a function of $(V_R - V_P)$. This is because changes of densities of states, as well as energetics, are important to the progress of chemical reactions. Therefore, curves resembling those in Figures 2 and 4 are almost always used in treating electron transfer reactions, but the coordinates are slightly different. The ordinate is the free energy, rather than the potential energy.[9,11,12] The abscissa is a reaction coordinate corresponding to the polarization and vibrational energy difference between reactant (D–A) and product (D$^+$–A$^-$ in this case) states arising in the molecules and in the solvent. Here D and A are the ET donor and acceptor, respectively. This reaction coordinate takes into account the contribution from all the degrees of freedom of the system, but reduces the system, effectively, to the crossing of two parabolas.

The inverse of the rate constant for electron transfer (as discussed in section I) is the time appropriate for transfer from a thermalized minimum in the left parabola of Figure 5 to a thermalized minimum in the right parabola. Figure 5 is essentially Figure 4 or Figure 2 generalized in three ways: (1) the initial and final states are no longer degenerate ($\Delta G^0 \neq 0$), (2) the abscissa is the (polarization energy plus vibrational energy) difference or reaction coordinate, and (3) the ordinate is the free energy, G, of the system.

Classically, ET nearly always requires traversing the barrier that intervenes between the reactant and product structures (interconverting reactants, D–A, and products D$^+$ – A$^-$). If

Contemporary Issues in Electron Transfer Research

J. Phys. Chem., Vol. 100, No. 31, 1996 **13151**
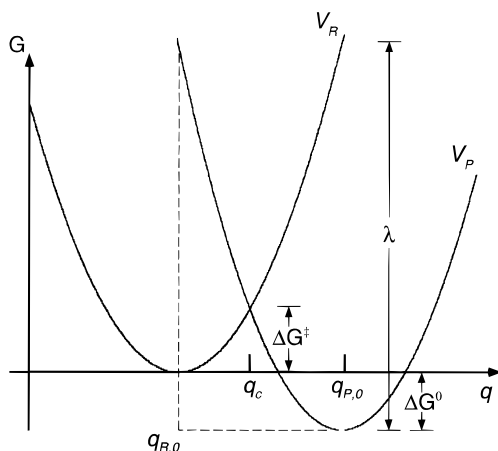
Figure 5. Diabatic free energy curves for an unsymmetrical electron transfer reaction.

nuclear tunneling is not important, this barrier can be calculated by straightforward algebra, as we will now show.

III. Transition State Theory for ET Rate Constants

Modern experimental study of electron transfer reactions really began with the availability of radioisotopes, so that self-exchange reactions, of the type

$$Fe(H_2O)_6{}^{2+} + {}^*Fe(H_2O)_6{}^{3+} \rightarrow$$
$$Fe(H_2O)_6{}^{3+} + {}^*Fe(H_2O)_6{}^{2+} \quad (III.1)$$
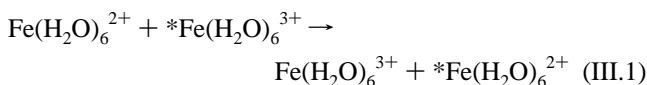
could be studied. The asterisk indicates a radioactive nucleus.[14,15] A number of workers, especially Marcus[9,11,12] and Hush,[16] studied the polarization response of the solvent, considered as a continuum dielectric, and the changes in polarization energy involved in localizing the electron on one of the two molecular units. This calculation requires computing the nonequilibrium free energy changes associated with transitions of the electron from being localized on one site to being localized on the other.[17−19] While analysis in terms of continuum electrostatics is fairly complicated, it can be understood simply by using the parabolas of Figure 2, 4, or 5.

The free energy barrier, $\Delta G^{\ddagger}$, is the difference between the crossing point and the bottom of the reactant free energy parabola. If we ignore entropy changes, the free energies become energies or potential energies. The barrier top, from the diabatic curves of Figure 5, occurs at position q_c (c for crossing) and is given by the condition

$$V_R(q_c) = V_P(q_c) \quad (III.2)$$

The potential energy curves now refer to the reactants (R or D−A) and products (P or D⁺−A⁻). Utilizing the definition of the potential energy curves, this condition is (with q_R and q_P the values of q at the R and P minima, respectively)

$$\tfrac{1}{2}f(q_c - q_R)^2 = \Delta G^0 + \tfrac{1}{2}f(q_c - q_P)^2 \quad (III.3)$$

We can solve this equation for the crossing point, obtaining

$$q_c = \frac{\Delta G^0}{f}\left(\frac{1}{q_P - q_R}\right) + (q_P + q_R)/2 \quad (III.4)$$

It is useful to define a fundamental physical quantity, the reorganizational energy λ. This quantity is indicated in Figure 5 and is defined mathematically by

$$\lambda = \tfrac{1}{2}f(q_R - q_P)^2 \quad (III.5)$$

Thus, the reorganizational energy increases with increasing separation between the minima corresponding to the initial and final states and with increasing stiffness or force constant.

The free energy barrier, or potential energy barrier if entropy changes are neglected, is given by

$$\Delta G^{\ddagger} = G_R(q_c) - G_R(q_R) = V_R(q_c) - V_R(q_R) \quad (III.6)$$

Given that the curve V_R is simply a parabola, this becomes

$$\Delta G^{\ddagger} = \tfrac{1}{2}f(q_c - q_R)^2 \quad (III.7)$$

Substituting for q_c from eq III.4, we obtain the simple form

$$\Delta G^{\ddagger} = \frac{1}{4\lambda}(\lambda + \Delta G^0)^2 \quad (III.8)$$

This expresses the barrier height or free energy of activation for crossing two diabatic curves in terms of the overall free energy of reaction, ΔG^0, and the reorganizational energy, λ. From the standard Arrhenius relationship between activation free energy and rate constant, the latter is given as

$$k_{ET} = A \exp\left[\frac{-(\Delta G^0 + \lambda)^2}{4\lambda k_B T}\right] \quad (III.9)$$

Here k_B is the Boltzmann constant, k_{ET} is the electron transfer rate constant, and A is a prefactor that depends on the frequency of crossing the barrier top. This fundamental formula is probably the most important relationship in ET rate theory.[9]

The reorganizational energy λ includes components from the vibrations of the molecules (inner-sphere or intramolecular reorganizational energy, Figure 1) and from the polarization changes in the dielectric solvent environment (outer sphere or solvent reorganizational energy, Figures 3 and 4). The standard estimate for the latter was obtained by Marcus by using a model in which reactants and products were modeled as spheres and the solvent as a dielectric continuum.[6,11,12] This form for the reorganizational energy is simply

$$\lambda_0 = (\Delta e)^2 \left\{\frac{1}{2a_1} + \frac{1}{2a_2} - \frac{1}{R}\right\}\left\{\frac{1}{\epsilon_\infty} - \frac{1}{\epsilon_0}\right\} \quad (III.10)$$

Here a_1, a_2, R, ϵ_∞, and ϵ_0 are respectively the radii of the donor and acceptor, the distance between their centers, and the optical frequency and zero frequency dielectric constants of the solvent. Δe is the amount of charge transferred. This dielectric estimate for the outer-sphere reorganizational energy makes specific assumptions with respect to geometry (two spherical reactants) and to equilibration. (The difference in the inverse dielectric constants relates to the fact that nuclear degrees of freedom cannot readjust instantaneously to the motion of the electrons and thus contribute to the barrier—this is a manifestation of the Born−Oppenheimer separation.)

In the case of self-exchange reactions, the driving force (negative free energy change, $-\Delta G^0$) vanishes, and eq III.9 becomes

$$k_{ET}(\Delta G^0 = 0) = A \exp\left[\frac{-\lambda}{4k_B T}\right] \quad (III.11)$$

Therefore, the activation free energy for the self-exchange case is simply one-fourth of the reorganization energy. The energy

for optical excitation from the R to the P potential curves is simply λ for this case.

IV. The Solvent Coordinate in Molecular Terms

For diatomics, the potential curves for electron transfer can be defined as a function of a simple coordinate, the internuclear separation. Similarly, for ET reactions we have shown in Figures 2 and 4 that the potential curves for simple electron transfers in which only one nuclear degree of freedom is important can be represented uniquely in terms of that degree of freedom.[20-22]

In the general case of electron transfer in solution, the solvent polarization coordinate completely determines the outer-sphere solvent contribution to the reorganizational energy, λ_0. Use of a dielectric continuum for the latter can problematic. The properties of individual solvent molecules—polarization, volume, etc.—are neglected. If hydrogen bonding is important, for example, different levels of hydrogen bonding in the initial, D−A, and final, $D^+−A^-$, states cannot be treated as part of a continuum solvation coordinate. They must be accounted for in molecular rather than continuum terms.[18] This is clearly shown in experiments with binuclear metal complexes, in which different degrees of hydrogen bonding completely dominate solvent effects.[23] It is also found if there are differing degrees of donor−acceptor interaction.

Computational attacks on the solvent reorganizational problem are challenging, but some important results have started to appear.[22] The first simulations involved actual calculation of the polarization coordinate discussed in section III and appropriate calculations of the free energy at each point.[13,24] Analysis of the resulting trajectory can be used both to compute the rate of ET (by analysis of how often the maximum is crossed) and for calculating the effective free energy curves. Simulations of this type have shown quite clearly[24] that the parabolic approximation developed by Marcus in the 1950s is remarkably accurate for model calculations such as the Fe^{2+}/ Fe^{3+} self-exchange reaction in aqueous solution (Figure 6).

Calculations of λ_0 by direct calculation of free energies by using a variation of the Onsager/Kirkwood cavity models have appeared.[17,18,25] Essentially, charge distributions are placed in dielectric cavities, and the free energies of interaction with the continuum environment are calculated. Important preliminary results include the fact that λ_0 is strongly distance dependent (this had been demonstrated experimentally previously),[26] λ_0 is generally larger for anions compared to cations, and λ_0 is quite sensitive to conformational and geometrical changes. Such computational studies of the reorganizational energy may be very important in understanding solvent control of ET reactions.

For reactions that do not occur in homogeneous solution, such as those at electrochemical interfaces or in proteins, defining the outer-sphere reorganizational energy in terms of a single coordinate becomes complicated. Clearly, the simple spherical reactant model in eq III.10 must be replaced by a more appropriate approximation. Both elliptical cavities[27] and cavities shaped to the electrostatic potentials of the donor and acceptor have been used.[17,28] The complication is in the nature of the geometrical conditions, or boundary conditions, at the electrochemical interface. In interfacial protein ET, only half of the real volume is occupied by solvent. There is a very hydrophilic region (dielectric constant close to 80, with mobile charges) and a hydrophobic region (dielectric constant closer to 2, with no mobile charges).

Understanding outer-sphere reorganizational energies in the latter two cases is quite complex. Continuum treatments have
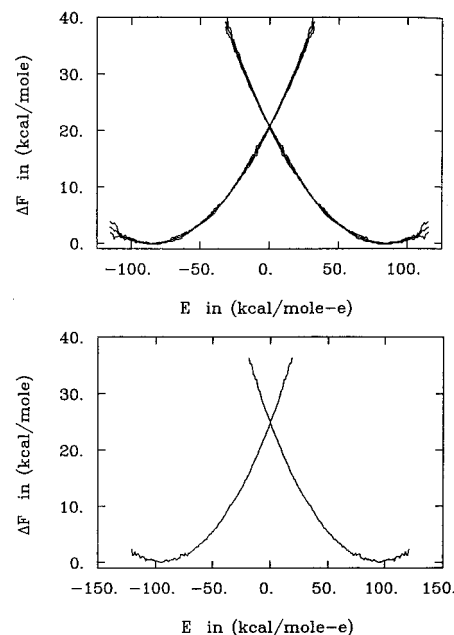
Figure 6. Simulated diabatic free energy function ΔF for Fe^{2+}/Fe^{3+} self-exchange with a fixed interionic separation of 5.5 and 6.5 Å, upper and lower graphs, respectively. For both, $T = 298$ K and the water density is 1.0 g cm^{-3}. Reproduced with permission from: Kuharski, R. A.; Bader, J. S.; Chandler, D.; Sprik, M.; Klein, M. L.; Impey, R. W. *J. Chem. Phys.* **1988**, *89*, 3248. Copyright 1988 American Institute of Physics.

begun to appear, with increasing levels of sophistication and adequacy.[17,25] The reaction coordinate can still be identified as the difference in polarization between donor and acceptor, as in eq II.4, but carrying out actual calculations for even simple molecular motions becomes complicated.

In polymeric, glass-forming, and protein environments, there is an additional complication due to the dynamics of relaxation, such that the full reorganizational energy may not be available on any given time scale.[29-31] In a frozen medium, λ_0 can be divided into a frozen part ($\lambda_{0,0}$) arising from dipole orientations and a nonfrozen part ($\lambda_{0,i}$) arising from translation-like lattice modes. $\lambda_{0,0}$ becomes part of ΔG^0, which increases emission energies in a glass compared to a fluid, for example. If relaxation of the medium occurs on the time scale of electron transfer, the two are coupled kinetically much as described in section XI for the coupling of ultrafast electron transfer to solvent dynamics.

The utility of eq III.10, in connection with eq III.9, in understanding electron transfer reactions in homogeneous solution is obvious from the great success that electron transfer rate theory has had in inorganic and organic solution phase chemistry. Much more needs to be done to account for specific solvent effects arising, for example, from H-bonding or donor−acceptor interactions. In addition, obtaining valid approximations analogous to eq III.10 for electron transfer at interfaces and in heterogeneous and slowly relaxing environments remains only a partly solved problem.

There is a considerable conceptual advantage to viewing solvent reorganization in terms of a collection of coupled oscillators (analogous to phonons in the solid state) in applying either classical or quantum theories. This allows for the introduction of entropic and temperature effects in a microscopically meaningful way, for example. Connecting and reconciling this molecular view with the molecular simulations and continuum treatments remains a challenge.

Contemporary Issues in Electron Transfer Research

J. Phys. Chem., Vol. 100, No. 31, 1996 **13153**
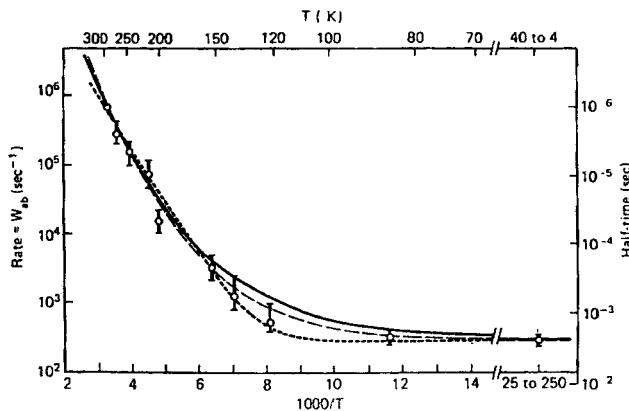
Figure 7. Comparison of theories with data on *C. vinosum* cytochrome oxidation. Data are points; various theoretical models yield the curves. Note the nonvanishing rate constant at low temperature. Reproduced with permission from: DeVault, D. *Quantum Mechanical Tunneling in Biological Systems*; Cambridge University Press: Cambridge, 1984. Copyright 1984 Cambridge University Press.

V. Quantum Mechanical Corrections: Vibronic Theory

Equation III.9 follows from transition state theory and is a highly useful relationship. It completely characterizes the electron transfer reaction in terms of three quantities: the prefactor A, ΔG^0, and the reorganizational energy, λ. It can be extended in an obvious way to include intramolecular vibrations by including an intramolecular reorganizational energy given by

$$\lambda_{\text{total}} = \lambda = \lambda_0 + \lambda_i \qquad (V.1)$$

$$\lambda_i = \sum_l \lambda_{i,l} = {}^1/_2 \sum_l f_l (\Delta q_{\text{e},l})^2 \qquad (V.2)$$

Here, the summation is over the coupled intramolecular vibrations. The contribution of the lth normal mode to the reorganization energy is given in terms of its force constant f_l and the change in equilibrium positions between the reactants and products, $\Delta q_{\text{e}} = q_{\text{P,e}} - q_{\text{R,e}}$.

But even with this generalization to include intramolecular effects, there are clearly problems with the theory. Perhaps the most important is the temperature dependence. Equation III.9 predicts a vanishing electron transfer rate constant at zero temperature. Experimentally, this is not observed. Data for the biological system *Chromatium vinosum*[32] are shown in Figure 7. Note that at low temperatures the rate constant is essentially temperature independent. It does eventually become activated (in agreement with the results for eq III.9) at high temperatures.[33] There are additional problems with the simple form of (III.9), including an excessively rapid falloff in k_{ET} with ΔG^0 and an exaggerated temperature dependence in the inverted region (section VII).

These difficulties arise because it is assumed that the barrier must be crossed. That is, no allowance is made for possible quantum mechanical tunneling through the barrier. This issue was addressed[2-8,10] by a number of workers,[34-39] who borrowed ideas from the polaron theory of charge transport in solids.[40,41] A particularly clear and applicable formulation was given by Jortner,[35] and we discuss it here briefly.[42] Complications arising from solvent dynamics (see section XI),[43-53] gating,[26,54-56] and multiple electronic states are discussed in other sections. Modes coupled to electron transfer must be treated as quantum mechanical if the spacing between the vibrational levels is large compared to thermal energies. Relationship V.3 provides a guide to which modes must be treated as quantum mechanical and which can be assumed classical. When $\hbar\omega \sim k_{\text{B}}T$, the

classical results are often reasonably accurate.

$$\frac{\hbar\omega_l}{k_{\text{B}}T} \gg 1 \qquad \text{quantum}$$

$$\frac{\hbar\omega_l}{k_{\text{B}}T} \ll 1 \qquad \text{classical} \qquad (V.3)$$

The necessity to introduce quantum effects is perhaps made clearest by inserting the harmonic oscillator vibrational energy levels within the potential curves of Figure 5, as shown schematically in Figure 8. As shown there, tunneling can occur optimally between the ground level in the reactant potential curve and the ninth vibrational level in the product curve. Tunneling must be taken into account in describing the rate constant. The extent to which tunneling plays a role depends on the extent of the vibrational overlap between the initial and final states.

It is historically interesting that Marcus derived part of the inspiration for his original treatment of ET from Libby's emphasis[57] on the constraints on the reaction dynamics caused by the Franck–Condon principle.[9]

The rate constant for electron transfer, from the golden rule of perturbation theory with the full Hamiltonian of the system, gives the ET rate constant, k_{ET}, as[2-10]

$$k_{\text{ET}} = \frac{2\pi}{\hbar}|\langle R|H|P\rangle|^2|\langle r_{\text{vib}}|p_{\text{vib}}\rangle|^2\delta(E_{\text{R}} - E_{\text{P}}) \quad (V.4a)$$

$$= \frac{2\pi}{\hbar}|\langle R|H|P\rangle|^2|\langle r_{\text{vib}}|p_{\text{vib}}\rangle|^2\rho(E_{\text{P}}) \qquad (V.4b)$$

$$= \frac{2\pi}{\hbar}|\langle R|H|P\rangle|^2(\text{DFWC}) \qquad (V.4c)$$

$$= \frac{2\pi}{\hbar}H_{\text{RP}}{}^2(\text{DWFC}) \qquad (V.4d)$$

Here the electron transfer rate constant is given first in terms of isolated levels for the reactant and products, then in terms of a density of states, $\rho(E_{\text{P}})$ of the product, and finally in terms of a density of states weighted Franck–Condon factor (DWFC). H_{RP} is the electronic matrix element that mixes the donor and acceptor states (see section VIII). The states $|r_{\text{vib}}\rangle$ and $|p_{\text{vib}}\rangle$ are vibrational states of reactant and product, respectively. H is the Hamiltonian of the entire system, and the matrix elements in eqs V.4a and V.4b are averaged over the full Hamiltonian of the system.

In the case of nonadiabatic ET, with the Condon approximation, this formulation is correct; for adiabatic ET, a more general prefactor is required.[1,58-64]

We focus now on the case of nonadiabatic ET. Using the polaron model, each electronic state is coupled with a number of vibrations, treated as harmonic oscillators with separation of nuclear and electronic coordinates assumed.[34-42,65-69] Under these conditions, one can formally write the total Hamiltonian of the system as

$$H = |R\rangle\langle R|\{E_{\text{R}}^0 + {}^1/_2\sum_l f_l(q_l - q_{\text{R},l})^2\} +$$
$$|P\rangle\langle P|\{E_{\text{P}}^0 + {}^1/_2\sum_l f_l(q_l - q_{\text{P},l})^2\} +$$
$$(|R\rangle\langle P| + |P\rangle\langle R|)H_{\text{RP}} \quad (V.5)$$

Here, the first term in braces is the energy represented by the left parabola of Figure 5, and the second set of braces is the
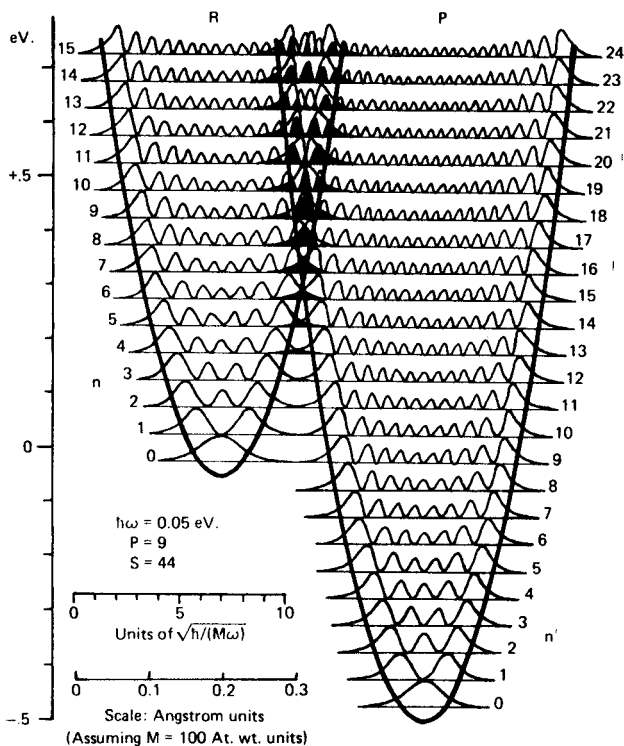
Figure 8. Schematic one-dimensional representation of the intersection between reactant and product vibrational levels. The optimal overlap of the $v = 0$ initial vibrational level is with the $v' = 9$ product level. Reproduced with permission from: DeVault, D. *Quantum Mechanical Tunneling in Biological Systems*; Cambridge University Press: Cambridge, 1984. Copyright 1984 Cambridge University Press.

same energy term in the right potential. E_R^0 and E_P^0 are respectively the energy origins for these states. They are characterized by the force constant f_l for the lth mode, whose displacement origin is $q_{R,l}$ and $q_{P,l}$ in the reactants and products, respectively.

This Hamiltonian is called the spin-boson model or the polaron model; it consists of two electronic states coupled with a large number of vibrational levels, which can be either quantum mechanical or classical. This model Hamiltonian has led to a great deal of analysis, and a number of attractive and useful forms for the rate constant have emerged.[2−10,42] If one specifies, in addition to the classical solvent motions, one coupled vibration characterized by frequency ω and the equilibrium displacement Δq_e, one can define the intramolecular reorganizational energy for this mode as

$$\lambda_i = (f/2)(\Delta q_e)^2 \qquad \text{(V.6)}$$

This can, in turn, be related to a related dimensionless quantity, the electron vibrational coupling constant or Huang−Rhys factor, as defined in eq V.7; μ is the reduced mass.

$$S = \frac{\lambda_i}{\hbar\omega} = \frac{f}{2\hbar\omega}(\Delta q_e)^2 = \frac{\mu\omega}{2\hbar}(\Delta q_e)^2 \qquad \text{(V.7)}$$

The generalization of eq III.9 for nonadiabatic ET for one coupled mode with $\hbar\omega \gg k_B T$, then becomes[35]

$$k_{ET} = \frac{2\pi}{\hbar} H_{RP}{}^2 \left(\frac{1}{4\pi\lambda_0 k_B T}\right)^{1/2} (FC) \qquad \text{(V.8)}$$

$$(FC) = \sum_{v'} \exp(-S)\frac{S^{v'}}{v'!}\exp\left\{\frac{-(\lambda_0 + v'\hbar\omega + \Delta G^0)^2}{4\lambda_0 k_B T}\right\} \qquad \text{(V.9)}$$

This rather complex looking expression can be fairly easily understood. The terms in front of the Franck−Condon (FC) factor are the frequency of electron transfer in the absence of a barrier; this contains H_{RP} and the classical density of states. The Franck−Condon factor itself consists of the sum over all possible vibrational overlap integrals between the initial vibrational level v and the final level v'. Each individual v' represents a separate $v = 0 \rightarrow v'$ reaction channel. Each separate exponential term in the sum is the population of molecules in the assembly having the required energy to undergo electron transfer with energy conservation through channel $v = 0 \rightarrow v'$. The sum is dominated by channels for which $|\Delta G^0| \sim \lambda_0 + v'\hbar\omega$, so there is a close energy match between the energy released (ΔG^0) and the sum of the reorganization energy and the initial product vibrational energy ($v'\hbar\omega$).

The quantal form of eq V.9 predicts a population in the product electronic state; additionally, it predicts that the exoergicity $|\Delta G^0|$ is distributed among the states of the quantum oscillator, with each final state v' having relative population $S^{v'}/v'!$. Very recent work[70−73] has detected vibrationally hot products following very rapid (picosecond) ET; such observations as well as vibrational levels, will permit more precise, quantitative theoretical formulations and detailed understanding of ET processes.

The form of (V.9) must be generalized when thermally excited, or otherwise excited, initial states are involved; closed form expressions similar to (V.9) emerge, but with sums over initial vibrations and FC factors between vibrationally excited reactant and product.[35] Very recent work in metal carbonyl charge transfer species has directly observed ET from specific vibrationally excited states.[71]

In eq V.9 it is assumed that the vibrational spacings and frequencies are the same before and after electron transfer. Changes in frequency in solvent modes are included in ΔG^0. The result in eq V.9 can be generalized to include thermal populations above $v = 0$ in the reactants; this introduces an additional temperature dependence. It can also be generalized to include many coupled vibrations explicitly.[2−10,42] This is often unnecessary. In the classical limit, individual reorganizational energies add up to give the λ_i of (V.2) (see section X). Similarly, it has been argued by many workers, and appears to be generally true, that the effects of quantum behavior can be subsumed by treating only a few modes quantum mechanically by mode averaging. Those few modes can represent averages of many contributions[42] With mode averaging, vibrations in a frequency range are averaged to give an averaged mode of S,

$$S = \sum_j S_j \qquad \text{(V.10)}$$

and effective frequency,

$$\hbar\omega = \sum_j S_j \hbar\omega_j / \sum_j S_j \qquad \text{(V.11)}$$

Appropriate grouping of the coupled vibrations allows for an accurate representation of their contributions, but resonance Raman spectroscopy permits[74−78] the mode by mode evaluation of λ (see section VII).

The single mode expression of eqs V.8 and V.9, along with its generalizations, cures most of the important inadequacies of the classical limit formula III.9. In particular, the temperature dependence is now correct: at low temperatures, with λ_0 negligible, quantum mechanical nuclear tunneling dominates and the temperature dependence is essentially flat. At high tem-

Contemporary Issues in Electron Transfer Research

J. Phys. Chem., Vol. 100, No. 31, 1996 **13155**
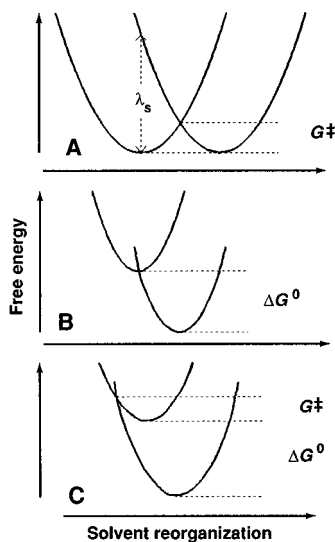
Figure 9. Schematic, one-dimensional representation of free energy surfaces relevant in nonadiabatic electron transfer reactions for (A) ($\Delta G^0 = 0$), (B) the special case where $-\Delta G^0 = \lambda_s$, and (C) highly exoergic reactions with $|\Delta G^0| > |\lambda_s|$. Reproduced with permission from: Closs, G. L.; Miller, J. R. *Science (Washington, D.C.)* **1988**, *240*, 440. Copyright 1988 American Association for the Advancement of Science.

Symbol	Compound	R_{DA}(Å)	k (sec⁻¹)	V (cm⁻¹)
Ste	Naph-Steroid-Biph	17.4	1.5×10^6	6.2
D-2,6-ee	Naph⁀Biph	14.0	5.0×10^7	30
D-2,6-ea		11.4	5.9×10^7	23
D-2,6-ae		11.0	2.3×10^7	13
D-2,6-aa		11.9	5.8×10^7	24
D-2,7-ee		12.5	2.9×10^8	54
D-2,7-ea		11.4	3.0×10^8	53
D-2,7-ae		10.9	1.75×10^8	38
D-2,7-aa		6.2	25×10^8	52
C-1,4-ee		11.8	1.6×10^9	128
C-1,4-ea		9.5	2.5×10^9	120
C-1,4-ae		9.3	0.45×10^9	50
C-1,3-ee		10.0	4.2×10^9	168

Figure 10 (Table 1). Distances, ET rates, and electronic interaction matrix elements in model compounds. Abbreviations: Naph, naphthalene; Biph, biphenyl; D, decalin; C, cyclohexane; e, equatorial; a, axial. Reproduced with permission from: Closs, G. L.; Miller, J. R. *Science (Washington, D.C.)* **1988**, *240*, 440. Copyright 1988 American Association for the Advancement of Science.

peratures, crossing over the barrier becomes important, until at very high temperatures the entire process becomes activated.

The vibronic theory also gives a far better representation of the temperature dependence in the inverted region, which is discussed in section VII. Figure 9 shows that tunneling barriers are expected to be substantially smaller in the inverted region than the normal region because the product potential curve is imbedded in the reactant curve. Vibrational overlap is higher, tunneling is more efficient, and only a very weak temperature dependence is seen in the ET rate constant. This is because there is little, if any, increase in vibrational overlap between v' and levels above.

In addition, the free energy dependence is no longer symmetrical as predicted by the classical result in eq III.9. The vibronic form of eqs V.8 and V.9 gives an exponential gap law in the inverted region and a Gaussian gap law in the normal region. The very important results on intramolecular electron transfer in bridged decalin and cyclohexane models[79] shown in Figure 10 convincingly show both the existence of the inverted region and the fact that the variation with ΔG^0 is not Gaussian in the inverted region.

VI. Vibrational Barriers and Reorganizational Energies

Changes in the number of electrons in molecules cause predictable changes in molecular structure. Reduction of $d\pi^6$ $Co(NH_3)_6^{3+}$ to $d\pi^5 d\sigma^{*2}$ $Co(NH_3)_6^{2+}$ adds two electrons to antibonding Co−N orbitals accompanied by a spin change. The Co−N bond lengths respond by increasing by 0.l8 Å. When polyaromatics are reduced to their radical anions, average C−C bond lengths increase because the electron is added to an antibonding π^* orbital.

These structural changes create a barrier to electron transfer. They can be resolved into linear combinations of the $3N - 6$ normal modes. The only modes that have to be considered are the ones that have a significant change in Δq_e, e.g., metal−ligand stretches for $Co(NH_3)_6^{3+/2+}$ and ring stretches for reduction of polyaromatics: they are the modes that undergo a change in equilibrium displacement Δq_e between redox states. If there is no change in symmetry, only totally symmetrical modes can be coupled.

While continuum theory involving dielectric polarization provides an effective and important beginning for treating the solvent reorganizational energy, the intramolecular reorganizational energy comes largely from the bond distance changes between reactant and product. We saw in section III that, within the harmonic approximation, the intramolecular reorganizational energy is the sum of contributions from the coupled vibrations and depends on their force constants and changes in equilibrium displacements. Extension of the result in eq V.9 to multiple vibrations shows that it is possible to consider the contribution of each normal mode to the reorganizational energy separately, and this provides a detailed and general analysis.

Evaluation on a mode-by-mode basis provides the means for complete evaluation of the vibrational barrier by application of a multimode version of eq V.9. Computationally, it requires knowledge of the normal coordinates, their frequencies, and their origin displacements between reactant and product. Such calculations have begun to appear,[65,80] as have estimates based on use of bond order/bond length relationships, one-electron (Huckel) type approximations, etc.

There are two standard approaches to obtaining the per-mode contribution to the reorganizational energy and barrier. The first is to combine a structural probe, such as X-ray crystallography or EXAFS, with a vibrational spectroscopy to obtain the frequencies.[81,82] This is obviously useful, since X-rays are sensitive to all geometrical changes (assuming that the hydrogens can be refined). There are limitations: structures are not always obtainable for both reactant and product, and when they are, structures obtained from a crystal may not always be relevant to a reaction in solution. Proper application also requires a normal-coordinate analysis. These limitations are quite severe, and only a few reorganizational energies have, in fact, been obtained in this way.

Figure 11. Coherent preparation and evolution of a vibrational wavepacket in photoinduced electron transfer. Reproduced with permission from: Doorn, S. K.; Blackbourn, R. L.; Johnson, C. S.; Hupp, J. T. *Electrochim. Acta* **1991**, *36*, 1775. Copyright 1991 Pergamon.

Important recent advancements in experimental resonance Raman spectroscopy, coupled with a reinterpretation of Raman cross sections in terms of time-dependent models,[83] have resulted in a number of elegant studies in which resonance Raman has been used to obtain the mode-by-mode analysis of λ_i and the vibrational barrier. Resonance Raman is an ideal probe if the optical equivalent of electron transfer can be observed. The only vibrations that are resonantly enhanced are those for which there is a change in equilibrium displacement, i.e., those that are coupled to the electron transfer. The theoretical connection[75−78,83−86] involves rewriting the perturbation theory sum-over-states expression in terms of an equivalent time-dependent expression,[75,83−85] with both a simple interpretation and some important computational predictions. Figure 11 illustrates the argument: the vibrational ground state of the initial electronic state (lower curve) is excited vertically and then evolves on the upper state. The time-dependent overlap of the vibrational wave function on the excited surface with that of the evolving ground state wave function, after half Fourier transform, gives the Raman cross section as

$$\sigma(\nu_i) = (\text{const}) \int_0^\infty dt \, \exp[(2\Pi i\Delta\nu - \Gamma)t]\langle\phi_f(0)|\phi_i(t)\rangle \quad \text{(VI.1)}$$

Here $\Delta\nu$, Γ, and ϕ_f and ϕ_i are respectively the difference between the incident frequency (ν_i) and the frequency of the resonant electronic transition, a damping factor, and the vibrational wave functions in the initial and final states. Time-dependent propagation methods are used to calculate Raman cross sections directly from time-dependent quantum mechanics within harmonic (or anharmonic!) models of the potential surfaces.

Under a well-defined set of required conditions, the ratio of Raman intensities for two coupled vibrations is given by[83]

$$\frac{I_1}{I_2} = \frac{\Delta_1^2\omega_1^2}{\Delta_2^2\omega_2^2} \quad \text{(VI.2)}$$

Here I_1, ω_1, and Δ_1 are respectively the intensity of the first vibrational mode in the resonance Raman measurement, its frequency (assumed the same for the ground and excited state), and its dimensionless displacement $\Delta_l = (\Delta q_{e,l})/(\hbar\omega_l/2f_l)^{1/2} = (2S_l)^{1/2}$. Use of the ω's from the resonance Raman spectrum gives relative values of Δ (and S) for coupled modes. These can be normalized, thus obtaining each individual contribution, from an analysis of line shapes.

This technique has now been pursued for a number of systems, including intramolecular ET in bridged binuclear metal

complexes,[52,75] as well as intermolecular ET reactions in complexes such as that between the hexamethylbenzene radical cation (HMB$^+$) and tetracyanoethylene radical anion (TCNE$^-$) studied by laser flash photolysis (VI.3). There are 11 coupled vibrations for this reaction.[76]

$$\text{HMB, TCNE} \xrightarrow{h\nu} \text{HMB}^+, \text{TCNE}^- \xrightarrow{k_{ET}} \text{HMB, TCNE} \quad \text{(VI.3)}$$

These results can be used in connection with a multimode version of eqs V.8 and V.9 to obtain important insights into the nature of ET. For example, it has been shown that the approximation made, based on mode averaging of vibrations having comparable frequencies, is generally adequate.[75,76,86] This is not a surprise since the ET rate constant is really an information-poor quantity derived from many different individual mode contributors. Detailed knowledge of the contributions is not required to obtain a good estimate of the rate constant.

Even with its successes, the resonance Raman analysis is no panacea. There are severe experimental limitations arising from the requirement to observe resonance enhancements from optical electron transfer bands. They are often of low intensity and convoluted with bands of higher intensity in the spectrum. Also, application of the time-dependent Raman analysis to molecules having complex electronic structures can be a formidable challenge.

VII. The Inverted Region

The classical result in eq III.9 predicts that, for a family of related reactants, k_{ET} should decrease with driving force ($-\Delta G^0$), reach a maximum at $-\Delta G^0 = \lambda$, and decrease as the driving force is increased further. This is illustrated in the energy coordinate curves in Figure 9. The predicted decrease, as $-\Delta G^0$ increases, may be counterintuitive but it exists experimentally and was predicted by Marcus in the early 1960s.[87,88]

This is the inverted region, one key to photochemical energy conversion and storage in natural photosynthetic systems and to the design of molecular assemblies for artificial photosynthesis.[89−92] A schematic example is shown in eq VII.1 in which light absorption gives an excited state that undergoes ET. Electron transfer creates transiently stored, oxidative and reductive equivalents at the oxidized donor and reduced acceptor. "Recombination" by back electron transfer (k_b) occurs in the inverted region and is inhibited because of the large driving force. This allows the redox equivalents to be transferred away from the initial site of excitation and utilized elsewhere. The role of the inverted region is paramount. The greater the energy stored, the greater the barrier to back electron transfer.[89]

$$\text{(VII.1)}$$

There have been some remarkably elegant molecules constructed with these principles in mind. One is the "pentad" (VII.2) in which free energy gradients and electron hopping separate the excited electron−hole pair over a long distance.[93] Another is a series of porphyrin assemblies in which the lifetimes of the transiently stored redox equivalents are on the millisecond time scale![94] There are clear implications in these results for the design of molecularly based energy conversion devices and for information storage.

Contemporary Issues in Electron Transfer Research

J. Phys. Chem., Vol. 100, No. 31, 1996 **13157**

Molecular chemiluminescence, the production of light in a chemical reaction, relies on the inverted region.[95,96] If there is sufficient driving force, the products of electron transfer include the excited state of one of the reactants. This is illustrated in the reaction between oxidized and reduced forms of $[Ru(bpy)_3]^{2+}$ in eqs VII.3. The reaction to give ground state $[Ru(bpy)_3]^{2+}$ is in competition, but slow due to the large driving force ($\Delta G^0 = -2.6$ eV).

(VII.2)

(VII.3)
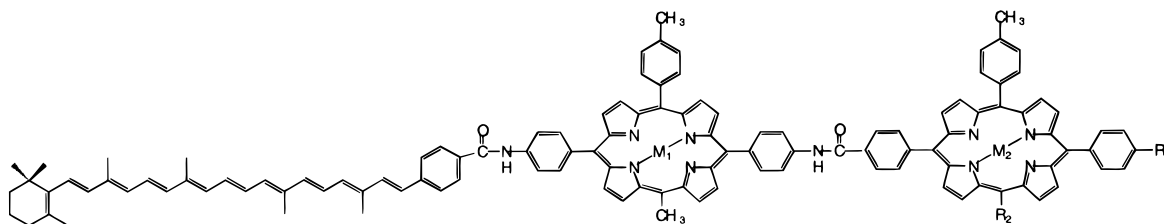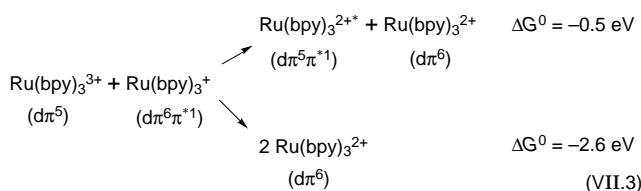
Although predicted by Marcus in the early l960s, the inverted region escaped detection for many years because experimental attempts were based on bimolecular electron transfer. As $-\Delta G^0$ is increased, the experimental rate constant (k_{obs}) changes from being activationally limited by ET (k_{ET}) to diffusionally limited (k_D). The three are generally related by

$$\frac{1}{k_{obs}} = \frac{1}{k_{ET}} + \frac{1}{k_D} \qquad (VII.4)$$

and if $k_{ET} \gg k_D$, $k_{obs} \cong k_D$.

Complications also arise from excited state formation (as in eq VII.3) and enhanced electronic interactions between untethered reactants free to undergo orientational changes to maximize electronic coupling.

Inverted behavior was first observed in frozen media.[97,98] In the first intramolecular example, pulse radiolysis was used to study electron transfer between a biphenyl radical anion donor and a series of organic acceptors (A) linked chemically by a steroid spacer, eq VII.5. In this study $-\Delta G^0$ was varied over a wide range, and the data were fit to eq III.9. Unequivocal evidence was found for a decrease in k_{ET} with driving force in the inverted region.[79,97]
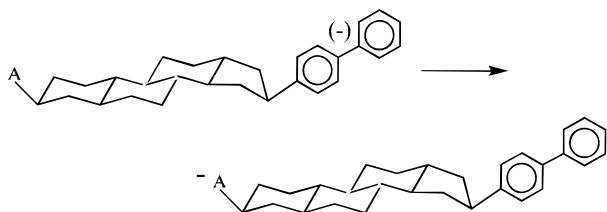
(VII.5)

The original description of the inverted region was classical and required thermal activation to the intersection between energy curves. The classical result in eq III.9 predicts that ln-(k_{ET}) should decrease parabolically with ΔG^0 in the inverted region. As noted in section V, the falloff is less than quadratic if there are coupled medium- or high-frequency modes, since acceptor vibrational levels well below the intersection are used and electron transfer occurs by nuclear tunneling. Inverted

electron transfer is similar to nonradiative decay of excited states in this regard.

The expression for k_{ET} in eqs V.8 and V.9 is general and also applies to the inverted region. In the limits, $|\Delta G^0| > \hbar\omega$ and $\hbar\omega \gg k_B T$, the sum over states result is adequately represented by eq VII.6, which is a form of the famous "energy gap law". (Here $1 + \gamma$ is the logarithm of ΔG^0 divided by $S\hbar\omega$.[99–102]) It predicts that the falloff in ln(k_{ET}) with driving force should be linear in ΔG^0. The solvent and coupled low-frequency vibrations treated classically ($\lambda_{i,L}$) are included in λ_0' ($=\lambda_{i,L} + \lambda_0$).

$$k_{ET} = \frac{2\pi}{\hbar} \frac{H_{RP}^2}{(\hbar\omega|\Delta G^0 - \lambda_0'|)^{1/2}} \times$$
$$\exp\left[-S - \frac{\gamma|\Delta G^0 - \lambda_0'|}{\hbar\omega} + \left(\frac{\gamma+1}{\hbar\omega}\right)^2 \lambda_0' k_B T\right] \quad (VII.6)$$

The predicted linear decrease is observed for the reactions in eq VII.7 studied by laser flash photolysis. Changes in driving force from $\Delta G^0 = -1.5$ to -2.3 eV caused k_{ET} to decrease by a factor of 30. In a related system a combination of kinetic and electrochemical measurements was used to show that eq VII.6 could be used to account for the solvent and temperature dependence (slight as expected) of electron transfer in the inverted region.[103,104]

$$[(4,4'-(X)_2bpy^{\bullet -})(CO)_3Re(py-PTZ^+)]^+ \xrightleftharpoons[k_{ET}]{h\nu}$$

$$[(4,4'-(X)_2bpy)(CO)_3Re(py-PTZ)]^+ \qquad (VII.7)$$

$$(X = CH_3O, CH_3, H, C(O)NEt_2, C(O)OEt)$$

py-PTZ
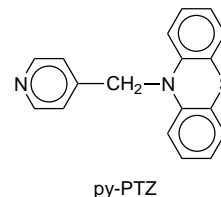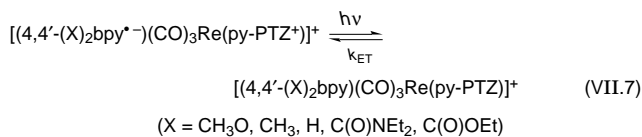
Similar observations have been made for electron transfer within contact radical ion pairs formed by laser flash photolysis of donor–acceptor complexes such as hexamethylbenzene and l,2,4,5-tetracyanobenzene (HMB, TCB), eq VI.3. The predicted linear decrease in ln(k_{ET}) with ΔG^0 was observed once variations in λ for the different reactants were included in the analysis.[105,106]

An increasing number of experimental examples prove the existence of the inverted region and the role of coupled medium- and high-frequency vibrations, but more are needed. A remaining issue, one shared with ET in mixed-valence compounds

(section IX), is the effect of electronic delocalization between the donor and acceptor. In this case, how do we describe the transition from electron transfer between weakly coupled donor−acceptor pairs to strong coupling and nonradiative excited state decay?

VIII. Distance Dependence of ET Rates: Theory, Experiments, and Pathways

Long-range (>5 Å) ET, especially in proteins, plays a central role in biochemistry, including photosynthesis and metabolism.[6,107−111] The rate of long distance electron transfer in proteins falls off rapidly (exponentially) with distance. This is indicative of an electron tunneling process. Many recent studies have been concerned with experimental measurements of the distance dependence of electron transfer rates in natural and modified proteins as well as synthetic peptides. At the same time a number of studies have appeared measuring rates for long- and intermediate-distance ET in non-peptide compounds.[79,92,112,113] Compounds in the latter class typically involve an electron donor and electron acceptor separated by a rigid spacer, yielding a donor and acceptor with a well-defined separation and orientation. Experimental studies on natural and synthetic systems have yielded data of great use in testing emerging theories for predicting ET rate constants from simple spectral and structural parameters.[5,108,114−121]

As described in section V, with weak donor/acceptor coupling, k_{ET} is predicted to vary with the square of the electronic coupling matrix element H_{RP} (eq V.4). The distance dependence of the solvent motion barrier is included in the DWFC. H_{RP} is predicted to fall off exponentially with distance because of the exponential radial character of the electronic wave functions of the donor and acceptor,

$$H_{RP} = V_0 \exp\left[-\beta \frac{(R - R_0)}{2}\right] \qquad (VIII.1)$$

V_0 is the donor/acceptor electronic coupling matrix element at van der Waals separation R_0. β is a constant that determines the rate of falloff of H_{RP} with distance.

For chemical examples in which the DWFC varies negligibly with R, the rate constant is predicted to reflect the distance dependence of H_{RP} as

$$k_{ET} = k_0 \exp[-\beta(R - R_0)] \qquad (VIII.2)$$

This is only true if λ_0 is small since it generally depends on distance as well (eq III.10).[6,26]

Many experimental studies have reported an exponential falloff in k_{ET} with distance in reasonable agreement with eqs VIII.1 and VIII.2, especially after the distance dependence of λ_0 is taken into account. These studies, which include organic and metal complex examples, proteins, and intermolecular electron transfer between donor and acceptors in frozen solutions, in general exhibit an exponential falloff of k_{ET} with β in the range 0.8−1.2 Å^{-1}. These values may be in error in some cases due to a limited set of experimental examples, failure to account for distance variations in λ_0 adequately, or conformational mobility. For differing classes of systems, β can vary substantially.[7]

There has been substantial theoretical interest in the nature of the electronic coupling between the donor and acceptor. In particular, this work has focused on the role of the intervening material (the bridging group) in modulating the effective electronic coupling. A broad array of modern electronic structure techniques have been applied to unravel the orbital pathways for coupling.[122−124] Coupling has been studied for saturated and unsaturated bridging groups as well as peptides. The relative importance of through-space and through-bond coupling has been examined, as have stereochemical effects (see Figure 10, for example). Constructive and destructive interference of various orbital pathways for electron and "hole" transfer by superexchange have also been studied. For systems with transition metals, the effect of spin−orbit coupling in mixing different spin states is a key ingredient in the superexchange coupling mechanism.

The generally good agreement between theory and experiment for the distance dependence of ET rate constants, even for complex systems, is highly encouraging and suggests that practical, quantitative methods for predicting the distance dependence of k_{ET} can be achieved in systems ranging from small rigid molecules to proteins.[125,126] Detailed theoretical calculations, however, suggest that the commonly found β values from 0.8 to 1.2 Å^{-1} may be deceptively simple. There can be many distinct electronic pathways that contribute to k_{ET} which can have a different distance and orientational dependences. There are theoretical and experimental reports of compounds having highly nonexponential distance dependences. In addition, an exceptionally shallow distance dependence of $\beta < 0.5$ Å^{-1} has been reported for electron transfer in peptides[127] and DNA.[128−130] These apparent exceptions to the usual experimental behavior are clearly interesting and will undoubtedly be investigated extensively in the future.

The conventional analysis of distance effects and of ET by eq V.8 relies on the Condon approximation and the assumption that H_{RP} is independent of molecular geometry for geometries near the equilibrium geometry for ET. The Condon approximation clearly fails in some cases. If H_{RP} is zero for electronic overlap, by symmetry in the equilibrium geometry of the reactants, it can become nonzero by vibronic mixing through non-totally-symmetrical modes. Of more important consequence are cases where electron coupling is significant, with H_{RP} approaching λ in magnitude. The assumptions of nonadiabatic transfer and the Condon approximation are then dubious, and results such as those in eqs V.8 and V.9 are no longer valid. This greatly complicates the calculation of ET rate constants and the spectroscopic interpretation of optical ET. This is an important area of future theoretical research.

IX. Mixed-Valence Chemistry

Mixed-valence compounds contain more than one redox state in the same molecule or molecular unit. There are many examples in biochemistry (e.g., iron−sulfur clusters), mineral chemistry (e.g., magnetite, Fe_3O_4), and molecular solids, $Sb^{III}Cl_3 \cdot Sb^VCl_5$.[131−135] The first designed mixed-valence molecule was the Creutz-Taube ion, $[(NH_3)_5Ru(pz)Ru(NH_3)_5]^{5+}$ (pz is pyrazine).[136] There are many examples in organic and metal complex chemsitry.

Mixed-valence complexes played an important early role in the study of intramolecular electron transfer. If there are localized redox states, the odd electron can be envisioned as in continual oscillation across the ligand bridge eq (IX.l).

$(NH_3)_5Ru^{III}(L)Ru^{II}(NH_3)_5^{5+} \rightleftharpoons (NH_3)_5Ru^{II}(L)Ru^{III}(NH_3)_5^{5+}$

L =   pz   4,4′-bpy   bpe

$$(IX.1)$$
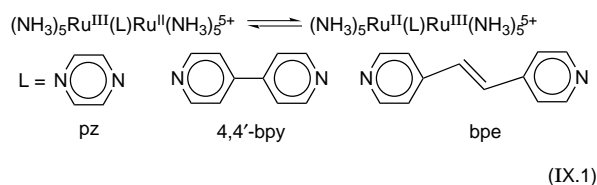
It has proven difficult to measure these interchange rate constants directly, but the optical analog can often be observed.

Contemporary Issues in Electron Transfer Research

J. Phys. Chem., Vol. 100, No. 31, 1996 **13159**

Symmetrical ($\Delta G^0 = 0$) and unsymmetrical ($\Delta G^0 \neq 0$) examples are shown in eq IX.2 and IX.3.

$$(NH_3)_5Ru^{III}(4,4'\text{-bpy})Ru^{II}(NH_3)_5{}^{5+} \xrightarrow{h\nu}$$
$$(NH_3)_5Ru^{II}(4,4'\text{-bpy})Ru^{III}(NH_3)_5{}^{5+} \quad \text{(IX.2)}$$

$$(NH_3)_5Ru^{III}(pz)Ru^{II}Cl(bpy)_2{}^{4+} \xrightarrow{h\nu}$$
$$(NH_3)_5Ru^{II}(pz)Ru^{III}Cl(bpy)_2{}^{4+} \quad \text{(IX.3)}$$
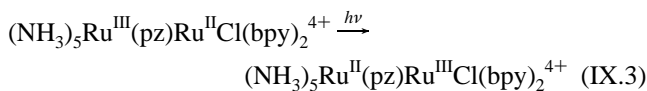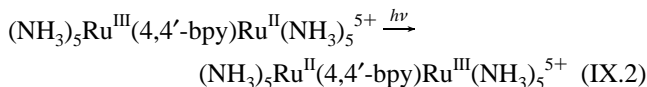
This special type of intramolecular charge transfer has been called intervalence transfer (IT) by Hush.

The electronic interaction between the donor (Ru^{II}) and acceptor (Ru^{III}) across the ligand bridge mixes electronic character and induces electron transfer. It also creates an electronic basis for inducing dipole-allowed, optical electron transfer, with the magnitude of the perturbation dictating the intensities of IT bands. For a Gaussian band shape in a two-level system, the delocalization energy arising by electronic coupling (H_{RP}) can be calculated[133] from the energy ($\bar{\nu}_{max}$ in cm^{-1}), molar extinction coefficient (ϵ_{max} in M^{-1} cm^{-1}), and bandwidth at half-height ($\Delta\bar{\nu}_{0,1/2}$, in cm^{-1}) by using eq IX.4; R is the electron transfer distance.[137]

$$H_{RP} \cong \frac{2.06 \times 10^{-2}}{R}(\epsilon_{max}\bar{\nu}_{max}\Delta\bar{\nu}_{0,1/2})^{1/2} \quad \text{(IX.4)}$$

The energy coordinate curves in Figure 5 illustrate the important energy relationships in intervalence transfer. They utilize mode averaging and a generalized coordinate which includes the coupled vibrations and solvent oscillations or librations treated classically as harmonic oscillators.

A number of important relationships between optical and thermal electron transfer can be derived from these curves. For symmetrical and unsymmetrical cases, the optical ET $\bar{\nu}_{max}$ is given by

$$\bar{\nu}_{max} = \lambda = \lambda_i + \lambda_0 \quad \text{(symmetrical)} \quad \text{(IX.5)}$$

$$\bar{\nu}_{max} = \Delta G^0 + \lambda = \Delta G^0 + \lambda_i + \lambda_0 \quad \text{(unsymmetrical)} \quad \text{(IX.6)}$$

These $\bar{\nu}_{max}$ are related to the corresponding free energies of activation for thermal electron transfer, ($\Delta G^\ddagger$), by (for $\Delta G^0 = 0$)

$$\Delta G^\ddagger = \frac{\bar{\nu}_{max}}{4} = \frac{\lambda}{4} \quad \text{(IX.7)}$$

and (for $\Delta G^0 \neq 0$)

$$\Delta G^\ddagger = \frac{(\bar{\nu}_{max})^2}{4(\bar{\nu}_{max} - \Delta G^0)} = \frac{(\lambda + \Delta G^0)^2}{4\lambda} \quad \text{(IX.8)}$$

The bandwidth is given by

$$(\Delta\bar{\nu}_{0,1/2})^2 = 16(\bar{\nu}_{max} - \Delta G^0)k_BT\ln 2 = 16\lambda k_BT\ln 2 \quad \text{(IX.9)}$$

These relationships open the door to using simple spectral measurements to assess the barrier to ET. Frequency changes in the coupled vibrations and solvent librations ($\hbar\omega \cong \hbar\omega'$) are included in ΔG^0 as a contribution to the entropic difference between states (if $\Delta\omega = |\omega - \omega'| \ll \omega, \omega'$).[138]

The classical approximation works reasonably well for low-frequency vibrations such as metal−ligand stretches near room temperature even though $\hbar\omega \sim k_BT$. It breaks down for aromatic ring stretching modes or CO or CN stretches where $\hbar\omega \gg k_BT$. They must be included explicitly in the vibrational barrier.

In symmetrical mixed-valence complexes, IT bands are typically found in the near-infrared (NIR) from l000 to 2000 nm (5000 to l0 000 cm^{-1}). They appear at lower energies for unsymmetrical complexes since $\bar{\nu}_{max}$ depends on ΔG^0 (eq IX.6). They tend to be broad and solvent dependent with molar extinction coefficients varying from a few M^{-1} cm^{-1} to thousands, depending on the ligand bridge. Small bridging ligands with accessible π and/or π^* levels such as O^{2-}, N_2, CN^-, and pyrazine promote strong electronic coupling by mixing ligand character into the metal $d\pi$ orbitals.

IT bands have been used to explore structural and solvent effects. In $[(bpy)_2ClRu^{III}(L)Ru^{II}Cl(bpy)_2]^{3+}$ (L = pz, 4,4′-bpy, bpe), R increases from 5.9 to l3.2 Å through the series. $\bar{\nu}_{max}$ was found to vary with $1/\epsilon_\infty - 1/\epsilon_0$ in a series of polar organic solvents and to increase with $1/R$ in CD$_3$CN.[139] Both are predicted by the dielectric continuum result in eq III.10, which assumes two noninterpenetrating spheres. Even better agreement was obtained with an ellipsoidal cavity model.[140]

A complication that has not always been appreciated is the existence of multiple IT transitions in the low-energy spectra. Low symmetries and spin−orbit coupling split the $d\pi$ orbitals, and there are overlapping transitions from each to the hole at Ru^{III}: $d\pi_1^2$, $d\pi_2^2$, $d\pi_3^2(Ru_a^{II}) \rightarrow d\pi_3^1(Ru_b^{III})$ (The labels a and b refer to the different metal ions across the bridge.) Only the lowest-energy transition $d\pi_3^2(Ru_a^{II}) \rightarrow d\pi_3^1(Ru_b^{III})$ is relevant to thermal electron transfer since the other orbital pathways give interconfigurational excited states at M(III), e.g. the transition $d\pi_1^2(Ru_a^{II}) \rightarrow d\pi_3^1(Ru_b^{III})$ gives $d\pi_1^1 d\pi_2^2 d\pi_3^2$ rather than $d\pi_1^2 d\pi_2^2 d\pi_3^1$.[141]

Dielectric continuum theory may work in some cases, but it fails if there are ligands such as NH$_3$ where H bonding can occur or CN$^-$ where donation of a lone pair leads to donor−acceptor interactions. These ligands have specific interactions with individual solvent molecules which can lead to novel phenomena.[142] For example, the Ru^{III} site in $[(NH_3)_5Ru^{III}(4,4'\text{-bpy})Ru^{II}(NH_3)_5]^{5+}$ is selectively solvated by DMSO in DMSO−acetonitrile mixtures. This maximizes H bonding at Ru^{III}, which is more acidic.[143] In $[(bpy)_2ClOs^{III}(4,4'\text{-bpy})Ru^{II}(NH_3)_5]^{4+}$ the Os(III)/Os(II) and Ru(III)/Ru(II) potentials are close, tuned by the difference in ligands. In acetonitrile−propylene carbonate mixtures, changes in the solvent actually cause Ru$^{II} \rightarrow$ Os^{III} electron transfer driven by enhanced solvent interactions at −Ru^{III}(NH$_3$)$_5{}^{3+}$.[144,145]

One of the reasons for interest in mixed-valence chemistry is the possible use of spectral measurements to calculate k_{ET} by using IT band measurements. $\Delta G^\ddagger$ and λ are available (using the spin-boson model) from the band maximum and the bandwidth (eqs IX.7, IX.8, and IX.9). H_{RP} is available from the integrated band intensity and eq IX.4. This would allow comparison between experimental and calculated rate constants, a goal that has remained largely elusive. Both measurements have been made in a bis(hydrazine) radical monocation with the hydrazine and hydrazinium redox sites rigidly fixed, separated by a 4.9 Å cyclic spacer. EPR line broadening measurements in acetonitrile at 25 °C gave $k_{ET} = 1.3 \times 10^8$ s^{-1}. An IT band appears at 6l4 nm ($\epsilon = 770$ M^{-1} cm^{-1}).[146]

A long-standing issue in mixed-valence chemistry is developing adequate models to describe the transition between localized and delocalized behavior. In $[(NH_3)_5Ru^{II}(4,4'\text{-bpy})Ru^{III}(NH_3)_5]^{5+}$ Ru^{III} and Ru^{II} are weakly coupled electronically. In $[(NH_3)_5Os^{II.5}(pz)Os^{II.5}(NH_3)_5]^{5+}$ the more compact bridge and greater radial extent of the 5d orbitals lead to strong electronic coupling

13160 *J. Phys. Chem., Vol. 100, No. 31, 1996*

Barbara et al.

and delocalization.[147] [(NH$_3$)$_5$Ru(pz)Ru(NH$_3$)$_5$]$^{5+}$ appears to be in between, at the crossover where $H_{RP} \sim \lambda$.[135] Another case is [(bpy)$_2$ClOs^{III}(px)Ru^{II}(NH$_3$)$_5$]$^{4+}$where there is strong electronic coupling but NIR and IR spectral markers for Os^{III}.[144,145] In these complexes the dπ orbitals along the pyrazine axis may be strongly coupled, but the highest level at Ru^{II} orthogonal and only weakly coupled to Os^{III}. Localization results if there is a residual solvent/vibrational barrier.

This and the transition between inverted electron transfer and nonradiative decay of excited states (section VII) are challenging areas for theoreticians and experimentalists alike. They are examples where the Condon approximation and the separation of electron and nuclear coordinates and the assumption of a two-site model may all be inadequate.[148,149] A non-Condon analysis has been applied to the Creutz−Taube ion but is not clear that the effects of symmetry, time scale, and spin−orbit coupling have been properly introduced.[149,150] For the experimentalist the challenge is to synthesize new examples where the subtleties in behavior in the localized to delocalized transition can be explored systematically.

X. Calculation of Rate Constants from Spectra

Application of the time-dependent Schrödinger equation and perturbation theory to transition rates between states gave the "golden rule" result in eq V.4. For light absorption the perturbation is the electromagnetic field of the incident light. Application of the Franck−Condon principle shows that the excited state is formed in the nuclear configuration of the ground state. Separation of the electronic and nuclear coordinates in the integral in eq V.4 gives rise to the integrated band shape equation in eq X.1 for absorption.[151] This assumes a single, coupled harmonic oscillator vibration of electron vibrational coupling constant S and quantum spacing $\hbar\omega$. It also assumes that $\hbar\omega = \hbar\omega'$ and $\hbar\omega \gg k_B T$. The solvent is treated classically and is included in the Gaussian distribution function. Changes in quantum spacing and densities of levels for the coupled solvent oscillations (librations) are included in ΔG^0 if $\Delta\omega = |\omega - \omega'| \ll \omega,\omega'$. $\vec{\mu}$ is the transition dipole moment, $\epsilon(\nu)$ the molar extinction coefficient at frequency ν, and c the speed of light. At low temperature,

$$\int \epsilon(\nu) \, d\nu =$$

$$\frac{2\pi N_A}{3000cn\hbar^2 \ln 10} \frac{|\vec{\mu}|^2}{(4\pi\lambda_0 k_B T)^{1/2}} \sum_{\upsilon'} (\Delta G^0 + \upsilon'\hbar\omega + \lambda_0) \times$$

$$\exp(-S)\frac{S^{\upsilon'}}{\upsilon'!} \exp\left[-\frac{(h\nu - (\Delta G^0 + \upsilon'\hbar\omega + \lambda_0))^2}{4\lambda_0 k_B T}\right] \quad (X.1)$$

The result is an integrated band shape equation in which the band is constructed from a series of vibronic lines. Each vibronic line is broadened by the solvent because there is a distribution of solvent polarizations around the ensemble of solutes. Any number of coupled vibrations can be included, as can "hot bands" arising from population of levels above $\upsilon = 0$ in the ground state. Equivalent expressions can be derived by the time-dependent formalism and generating function techniques. For a Gaussian-shaped absorption band in the classical limit, the results in eqs IX.4, IX.5, and IX.8 are obtained. Note that absorption spectroscopy, like ET itself, is controlled by Franck−Condon factors, so that the vibrational parts of the expressions X.1 and V.9 are very similar.

Similarly, the spectral band shape equation for emission in eq X.2 can be generalized to include any number of coupled

vibrations. $I(\nu)$ is the emitted intensity. At low temperature,

$$\int I(\nu) \, d\nu =$$

$$\frac{8\pi N_A}{3c^2\hbar^3} \frac{|\vec{\mu}|^2}{(4\pi\lambda_0 k_B T)^{1/2}} \sum_{\upsilon} (\Delta G^0 + \upsilon\hbar\omega + \lambda_0)^3 \times$$

$$\exp(-S)\frac{S^{\upsilon}}{\upsilon!} \exp\left[-\frac{(h\nu - (\Delta G^0 + \upsilon\hbar\omega + \lambda_0))^2}{4\lambda_0 k_B T}\right] \quad (X.2)$$

For states that are connected by electron transfer, if absorption or emission can be observed, the similar Franck−Condon factors result in a happy coincidence between the spectral band shape equations and those for the vibrational barrier to electron transfer. Both are coupled to the same vibrations and solvent librations and both are parametrized in S, $\hbar\omega$, λ_0, and ΔG^0.[41,152] The classical results in section IX for intervalence transfer in mixed-valence compounds can be generalized to calculate barriers, integrated band intensities used to calculate H_{RP} (eq IX.4), and k_{ET} calculated by using eqs V.8 and V.9.[133,153]

For emission in a two-level system, a useful relationship exists between H_{RP} and k_r, the rate constant for radiative decay. It is given in eq X.3. $\langle\bar{\nu}^{-3}\rangle$ is the average of the inverse cube of the emission energy. n is the index of refraction, R is the electron transfer distance, and $\bar{\nu}_{max}$ is the maximum for the underlying absorption band.

$$H_{RP}^2 = 1.39 \times 10^5 \left(\frac{\bar{\nu}_{max}}{nR}\right)^2 \langle\bar{\nu}^{-3}\rangle k_r \quad (X.3)$$

Experimental implementation of these powerful relationships between spectral measurements and dynamical quantities (k_{ET}) can be difficult to achieve. Charge transfer spectra are broad (because of coupling to the solvent), and there are usually many coupled vibrations. In the absence of vibronic structure it is impossible to obtain unique S and $\hbar\omega$ values for the individual vibrations. The adavantageous mode by mode description offered by resonance Raman was mentioned earlier (section VI). However, the acquisition and analysis of Raman excitation profiles are tedious. While mode averaging can be helpful, several difficulties occur in actual comparison of k_{ET} and spectral properties.

Even with mode averaging, analysis of absorption spectra is often problematical. Complications arise from spectral overlap and masking of the appropriate band by others of higher absorptivity. Mixed-valence compounds are an exception, with their intervalence transfer bands often appearing in the near infrared (section IX). In organic donor−acceptor complexes and intramolecular charge transfer molecules such as (*N,N*-dimethylamino)benzonitrile, charge transfer bands often appear at lower energy than other bands or as shoulders on higher energy features. Charge transfer excitation in these molecules leads to twisted intramolecular charge transfer (TICT) excited states in which there is a considerable charge separation because of the mutually perpendicular conformations of D$^+$ and A$^-$.[154,155]

 (X.4)
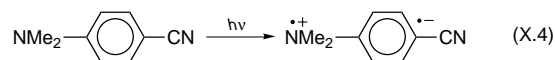
The most interesting cases are those where calculated and measured rate constants can be compared directly. An example is shown in eq VII.7 where ligand-to-ligand charge transfer bands, the optical reverse of the electron transfer, were used to calculate $H_{RP} \sim 40-60$ cm^{-1}. Electrochemical measurements gave ΔG^0, and γ and $\hbar\omega$ in eq VII.6 were obtained by kinetic

Contemporary Issues in Electron Transfer Research

J. Phys. Chem., Vol. 100, No. 31, 1996 **13161**

1

2
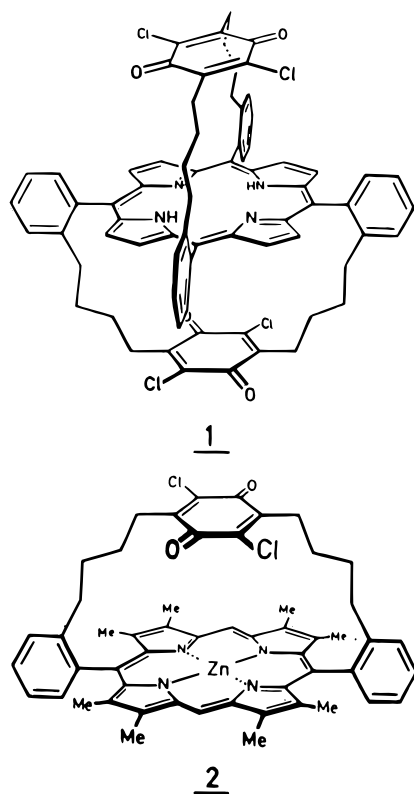
Figure 12. Structures of the porphyrin−quinone cyclophanes. Reproduced with permission from: Pollinger, F.; Heitele, H.; Michel-Beyerle, M. E.; Anders, C.; Futscher, M.; Staab, H. A. *Chem. Phys. Lett.* **1992**, *198*, 645. Copyright 1992 North-Holland.

and spectral analysis. Calculated and experimental values of k_{ET} agreed to within a factor of 10.[156] In analyzing these data, it was necessary to use the quantum results in eqs V.8 and V.9 or eq VII.6 because medium-frequency ring stretching modes are coupled to electron transfer. The classical results in eqs IX.5−IX.8 are inadequate.

It is easier to analyze emission spectra than absorption spectra because emission is rarely observed from more than one state, and there is no problem with spectral overlap. Emission is only expected in the inverted region where the energy curves are imbedded. It has been applied to back electron transfer in contact radical ion pairs such as the one in eq VI.3. Emission spectral analysis in this case gave λ_v $(=S\hbar\omega)$, λ_0, and ΔG^0. H_{RP} was calculated from k_r. The agreement between calculated and experimental values was remarkable[105,106] with (for example) $k_{obs} = 7.7 \times 10^9$ s^{-1} and $k_{calc} = 5.4 \times 10^9$ s^{-1} in 1,2-dichloroethane at room temperature. It was also possible to account for the solvent dependence of k_{ET} quantitatively. These results are reminiscent of those obtained in earlier studies on nonradiative decay in metal-to-ligand charge transfer (MLCT) excited states of polypyridyl complexes of Ru^{II} and Os^{II} (eq X.5). In those cases a similar level of quantitation was obtained.[157]

$$Os^{III}(bpy^{\bullet-})(bpy)_2{}^{2+} \rightarrow Os^{II}(bpy)_3{}^{2+} \qquad (X.5)$$
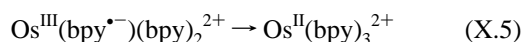
The agreement between experiment and theory reached in these cases is impressive. It will be interesting to apply resonance Raman spectroscopy to obtain mode-specific information routinely. Many more examples need to be studied as well. They will establish generalities and lead to new phenomena with the available theory as a benchmark. The benchmark itself is in need of an upgrade to treat cases where the Condon approximation fails and electron and vibrational coordinates are

mixed. These cases exist, and many more will appear once we have the tools to describe them properly.

XI. Ultrafast Electron Transfer and Nonequilibrium Electron Transfer Effects

Important insight into the molecular dynamics of ET reactions is being achieved through recent theoretical and experimental studies on ultrafast ET.[46,50,73,84−86,158−173] The systems under investigation include photosynthetic reaction centers, metallointercalators in DNA,[174,175] and intermediate size intramolecular ET examples such as the following model reactions,[51−53,72,176−183]

$$(NH_3)_5Ru^{III}-NC-Ru^{II}(CN)_5{}^- \underset{k_{ET}}{\overset{h\nu}{\rightleftharpoons}} (NH_3)_5Ru^{II}-NC-Ru^{III}(CN)_5{}^- \quad (XI.1)$$

(XI.2)
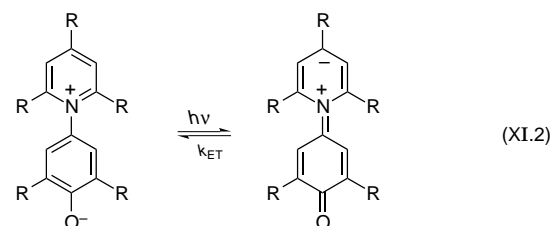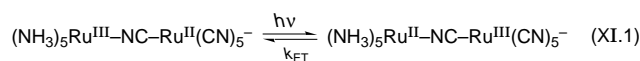
and the compounds in Figure 12.

Intermolecular ET in donor/acceptor complexes has also been extensively investigated by ultrafast spectroscopy, such as[158,184−188]

(XI.3)

(XI.4)

(XI.5)
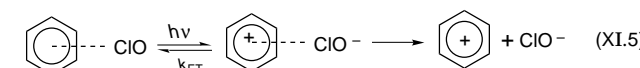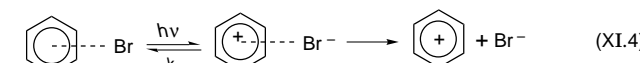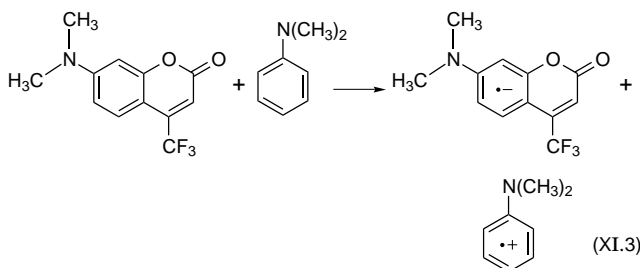
Ultrafast ET reactions are especially sensitive to nonequilibrium dynamical effects involving nuclear motions of the reactants and the solvent.[49,50,176,182,189] Such effects can represent a breakdown of the quasi-equilibrium picture of nonadiabatic and transition state theories for thermal ET kinetics.[43,45,47,169,190−197] In addition, nonequilibrium dynamical effects offer a direct contact with state-of-the-art methods for molecular simulations of chemical reactions in solution including emerging theories for quantum chemical dynamics in the condensed phase.[198−211]

Nonequilibrium effects involving solvation in ET reactions have been investigated broadly in recent years. It is now known that the solvent has a distribution of relaxation processes, involving both (1) inertial (free streaming) motion of the solvent (uncoupled solvent molecules) on the tens of femtosecond time scale and (2) slower diffusional solvent motions which can range from one to several picoseconds for ordinary solvents at ambient temperature. Solvation dynamics have been extensively measured by the transient Stokes shift method which uses polar fluorescent probe molecules in polar solvents, as well as molecular simulation methods, and, more recently, molecular theories of solvation dynamics. These studies have offered a unique view of chemical dynamics in solution and involved a

detailed and extensive contact between theory and experiment in the structure and dynamics of solutions.[49,161,212-222] The generally good agreement between theory and experiment for polar solvation dynamics is encouraging.

Much of the earlier theoretical work on dynamic solvent effects on ET rates was based on models of ET reactions that ignored the role of reactant vibrational modes and assumed that the solvent motion is entirely diffusional. Such models predict that k_{ET} should correlate with the diffusional solvation time (τ_s),

$$k_{ET} \approx \frac{1}{\tau_s} \exp\left(\frac{-\Delta G^{\ddagger}}{RT}\right) \qquad (XI.6)$$

For small barrier ET reactions ($\Delta G^{\ddagger} < k_B T$), the rate constant is predicted to be close to the rate constant for solvation dynamics, i.e.

$$k_{ET} \sim 1/\tau_s \qquad (XI.7)$$

This corresponds physically to the limit in which the time scale for ET is controlled by motion of the solvent. One experimental example that apparently corresponds to this limit is the excited state charge separation of the S_1 state in 9,9'-bianthryl,[223,224]

$$A-A \xrightarrow{h\nu} A-A^* \xrightarrow{h_{ET}} A^+-A^- \qquad (XI.8)$$

where A signifies an anthracene ring.

There are a number of experimental examples for which the electron transfer rate constant is faster than diffusional solvation dynamics. One of the earliest reported examples is intramolecular excited state charge separation in ADMA,[225] which far exceeds the time scale for diffusional solvation dynamics.

$$D-A\ (S_0) \xrightarrow{h\nu} D-A\ (S_1) \xrightarrow{k_{ct}} D^+-A^-\ (S_1)$$

$$(XI.9)$$
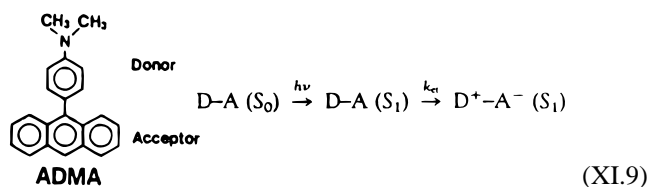
Other reported examples include intervalence transfer in a Ru^{II}-Ru^{III} mixed-valence complex (XI.1),[52,180] intermolecular electron transfer in Nile Blue with electron-donating solvents,[158] and charge separation in certain bridged donor/acceptor compounds (Figure 12).[159,189]

These various examples show that there must be fast nuclear motions capable of promoting ET and, subsequently, of accepting the energy generated in the ET process. One possible source is the inertial component of solvation dynamics. It has been argued that inertial solvational dynamics may be effective in promoting ET reactions, especially in aqueous environments.[52,212] This coupling would obviate any correlation of k_{ET} with diffusional solvation time scales.

A dramatic experimental example of an ET process where inertial solvation dynamics have been implicated is the Ru^{II}-Ru^{III} mixed-valence system in eq XI.1. Femtosecond pump–probe spectroscopy reveals multiple time scales for reaction and relaxation (Figure 13). The actual ET process occurs on the 80 fs time scale in H$_2$O which is much shorter than the time scale for diffusional solvation dynamics (~500 fs). An observed isotope effect of 1.4 on the electron transfer rate constant suggests that inertial solvation dynamics are directly coupled to ET. Interestingly, the time scale for ET is still slower than that predicted for inertial relaxation of H$_2$O ($\tau_{inertial} \sim 20-30$ fs), suggesting that electron transfer is not simply controlled by inertial solvation dynamics.
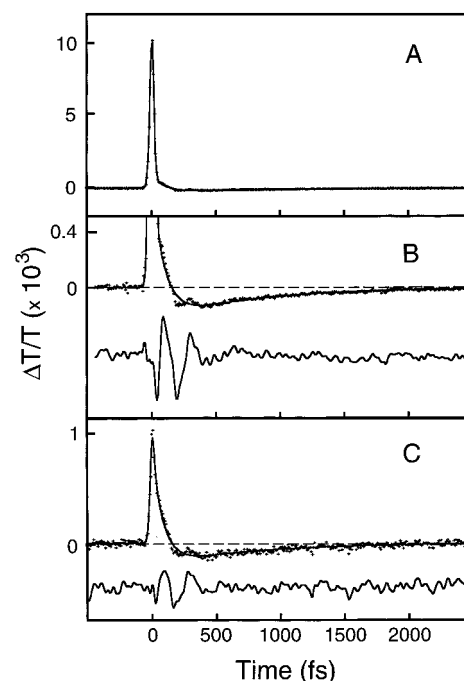
Figure 13. (A) Femtosecond absorption transient for (XI.1) in water obtained with pump and probe wavelengths 795 nm. Relative orientation of the pump and probe polarizations is parallel. The solid line corresponds to best fit of the the instrument response convolved with two exponentials. Kinetics and amplitudes were insensitive to a factor of 5 reduction in pump power. (B) Expansion of (A) revealing the presence of the ground-state bleach and longer time absorption. Analysis of the transient resulted in a back electron transfer time of 85 ± 10 fs and ground-state absorption decay time of 880 ± 160 fs. The residual difference between the fit and the data is given by the lower line demonstrating the oscillatory response of the sample. (C) Transient obtained with perpendicular pump and probe polarizations. Reproduced with permission from: Reid, P. J.; Silva, D.; Barbara, P. F.; Karki, L.; Hupp, J. T. *J. Phys. Chem.* **1995**, *99*, 2609.

Since k_{ET}^{-1} is substantially shorter than τ_s in eq XI.1 and related examples, the diffusional motions of the solvent are effectively frozen during the ET process. Further, this causes an increase in the effective ΔG^0 since ET occurs with solvent diffusional motions essentially frozen in a nonequilibrium distribution. A similar effect exists for slower ET in a glass or other rigid media where these motions are frozen (section IV). Thus, nonequilibrium solvent effects must be considered in detail for ultrafast electron transfers.

Besides nonequilibrium solvent effects, a variety of nonequilibrium intramolecular vibrational effects have been observed for ultrafast electron transfer reactions. For example, for reaction XI.1 and Figure 13, the electron transfer is sufficiently rapid that the products are prepared with a hot vibrational distribution which is apparent in the femtosecond pump–probe data. A ~ 1 ps component is observed due to vibrational cooling of the hot products of the ET reaction. This has also been observed for this reaction by transient vibrational spectroscopy.[72,183]

A second type of nonequilibrium vibrational effect that has been observed in ultrafast experiments on electron transfer is an oscillatory component of the pump–probe signal due to coherent intramolecular vibrational excitations of the reactant and product. This is demonstrated in Figure 13 for the reaction XI.1. The frequency of the oscillations corresponds to a vibrational frequency in the Ru^{II}Ru^{III} form.[75,226] Coherent vibrational effects on ET reactions is at the forefront of ET research. Coherent oscillations have been observed in a broad

Contemporary Issues in Electron Transfer Research

J. Phys. Chem., Vol. 100, No. 31, 1996 **13163**

range of intramolecular and intermolecular ET reactions, including photosynthesis.[52,186,224−231]

Coherent vibrational effects have been predicted to result from several different sources. Due to the short duration of the optical pulse, it can impulsively excite a coherent vibrational wave packet which may influence the ET kinetics, perhaps resulting in an oscillating "rate" of ET. Indeed, an ultrafast reaction can in principle create a coherent vibrational excitation in the products under certain circumstances.[84,232] In addition, the optical excitation pulse can create vibrational coherence due to resonance impulsive stimulated Raman scattering, which is a general phenomenon not necessarily related to the ET process. The latter process is apparently responsible for the coherent oscillation in the RuRu data.[52] It is still an open question whether coherent vibrational effects can play an important role in modulating ET rates.

Nonequilibrium vibrational effects must also be considered in relation to the dynamic solvent effect, which was discussed above. Theory predicts that vibrational degrees of freedom can significantly reduce the magnitude of the dynamic solvent effect; this has been confirmed experimentally.[176,178,191,233−235] A particularly dramatic example is the betaines (eq XI.2), where the ET reaction can be controlled by solvation dynamics or vibrational/electronic factors depending on the time scale for solvation dynamics.[50,236−238]

Inverted regime ET reactions (see sections VI and VII) are closely related to radiationless transitions of excited polyatomic molecules (e.g., internal conversions and intersystem crossing).[102,239,240] These typically occur far from the crossings of the ground and excited state surfaces, and substantial amounts of energy are deposited in vibrational and solvent degrees of freedom during the radiationless decay. Historically, condensed phase radiationless transitions are discussed in terms of separate promoting and accepting vibrational modes. The type of promoting mode differs depending on the mechanism for the radiationless decay. For example, for internal conversion processes that do not involve substantial charge transfer, the promoting mode is assumed to be a non-totally-symmetric mode of the molecule which induces vibronic mixing; this is necessary to overcome the symmetry constraints on the electronic mixing. For electron transfer reactions (in the weak donor/acceptor coupling limit) the promoting mode is assumed to be solvent degrees of freedom that cause fluctuations of the energy gap of the localized charge transfer states, i.e., the solvent coordinate.

Despite the tremendous success of the weak coupling model for electron transfer reactions, there are reasons to consider the range of validity of such an approach.[69] For example, for ET in water, the solvent degrees of freedom are the likely promoting modes, but some of the solvent modes are of sufficiently high frequency that they should be treated quantum mechanically, in contrast to the usual electron transfer model. A second area of concern is the possible role of vibronic mixing which is absent in the rudimentary electron transfer model. In general, the range of validity of the weak coupling approximation is a complex problem due to the many nuclear degrees of freedom with a broad range of vibrational frequencies and reorganization energies. Fortunately, theoretical methods are rapidly developing for examining theses issues by mixed quantum mechanical/ classical molecular simulation. These methods are being applied in a number of laboratories to examine the underlying physical bases of ET in molecular terms.[84,198−203,241,242] Eventually, this approach may lead to practical calculation procedures for modeling and predicting inverted regime rates using input from electronic structure calculation methods for the reactants and
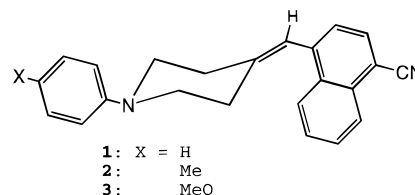
Figure 14. Structure of the D−B−A systems investigated for vapor-phase intramolecular ET. Reproduced with permission from: Verhoeven, J. W.; Scherer, T.; Wegewijs, B.; Hermant, R. M.; Jortner, J.; Bixon, M.; Depaemelaere, S.; De Schryver, F. C. *Recl. Trav. Chim. Pays-Bas* **1995**, *114*, 443. Copyright 1995 Elsevier.
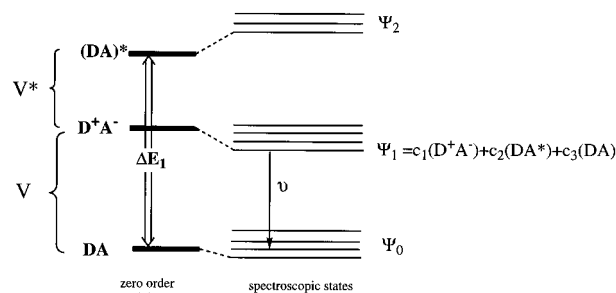
Figure 15. Three-state model for mixing of the charge transfer state with both the ground state and the lowest locally excited state in donor−acceptor systems. Reproduced with permission from: Verhoeven, J. W.; Scherer, T.; Wegewijs, B.; Hermant, R. M.; Jortner, J.; Bixon, M.; Depaemelaere, S.; De Schryver, F. C., *Recl. Trav. Chim. Pays-Bas* **1995**, *114*, 443. Copyright 1995 Elsevier.

molecular theories of solutions for the solvent. This would represent a breakthrough in the quantitative modeling of ET reactions.

XII. Gas Phase Electron Transfer: Harpooning and Energetics

While the dominant interest in electron transfer reactions certainly is in the condensed phase, a great deal can be learned by studying such reactions in vapor, free from the complications of solvent dynamics, solvent polarization, and solvent energetics. Recent work[243−247] on bridged donor/acceptor compounds has brought considerable insight into the nature of the energetics, the gating of ET reactions by geometric rearrangements far beyond the harmonic approximation, and the energetics of the ET reaction. A characteristic example is shown in Figure 14. Understanding the optical excitation in this species requires not the two-level model usually considered in the Mulliken theory of charge transfer absorption, but rather a three-level model.[246] The three levels are DBA, D^+BA^-, and (DBA)* (Figure 15). Here the DBA triad is a donor−bridge−acceptor system (by which we mean that the electron localization sites are really on the donor and acceptor moieties and that the bridge simply acts as a linker and, possibly, an electron coupler), and the three states are the neutral ground state, the charge transferred state, and the optically excited state.[248]

Within a chromophore such as that in Figure 14, optical excitation prepares the (DBA)* state. As the kinetic scheme in Figure 15 shows, this state can decay in several ways: it can undergo radiative or nonradiative recombination to the DBA ground state, or it can transfer charge to form the D^+BA^- state.

For the charge transfer exciplex (the D^+BA^-) to form, the free energy change must be negative for formation from the initially excited state. This free energy change can be given in terms of a variation of the Rehm−Weller equation as[246,249]

$$\Delta G = \Delta G_\infty - e^2/R_{+-} \qquad \text{(XVII.1)}$$
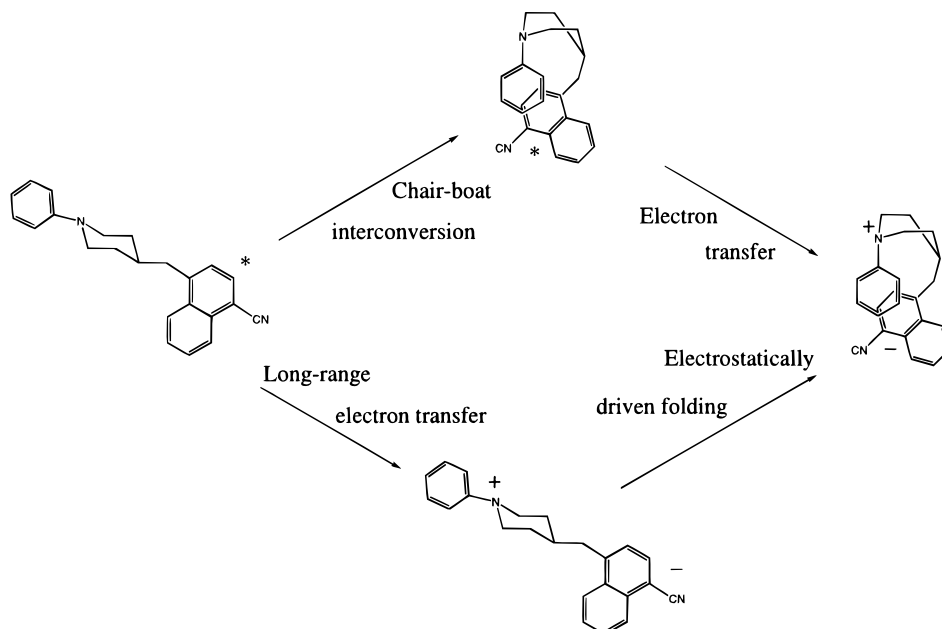
Figure 16. Two possible mechanisms for intramolecular exciplex formation. Reproduced from: Wegewijs, B. Thesis, University of Amsterdam, 1994.

Here the first term is simply the energy difference between the two states in the absence of Coulomb interaction (which can, for example, be estimated using electrochemical reduction data or photoemission and electron capture data), while the latter term represents the Coulomb attraction between cation and anion; we have idealized this interaction as the interaction of two electronic point charges a distance R_{+-} apart.

Experiments have shown conclusively that[243-246] if sufficient energy is deposited in the photoexcited state that the Rehm–Weller equation predicts downhill free energy transfer, the ET reaction will occur with a probability that depends on the geometric separation across the bridge. Upon forming the charge transferred exciplex, however, the energy clearly will be substantially reduced if the bridge structure changes its geometry, to bring the cationic donor and the anionic acceptor closer to one another. In this sense, the back electron transfer reaction, re-formation of the DBA state from the D$^+$BA$^-$ state, proceeds by a variant of the "harpooning" mechanism, originally developed for reactions of a very different type.[250] That is, the installation of a flexible (as opposed to a rigid) bridge permits harpooning of the cation by the anion, such that the molecule distorts to bring them together, which facilitates subsequent electron transfer processes to form the ground state (Figure 16).

Extended studies of such transfers in the vapor phase have proven the energetics, the appropriateness of the Rehm–Weller equation, the mechanism of harpooning, and the validity of the three-level model.[243-246,248] In this series of reactions, the energetics can be finely enough tuned that effects of variations in the inner-sphere reorganization energy may well determine whether the reaction proceeds or not. Such tuning has not yet, to our knowledge, been done. It would be very useful to do so, because it could provide a straightforward link between inner-sphere reorganization energy and rate, in the absence of complications from solvent behavior. This, in turn, would permit some fairly exacting conclusions to be drawn about the appropriateness of various methods for evaluating reorganization energies.

XIII. Conductive Polymers

Many examples of extended delocalized electronic systems exist in organic chemistry; the polyacenes and the conjugated linear polyenes, from butadiene to hexatriene, octatetraene, and so forth, are classic examples. When these conjugated systems become long enough, they can be considered as oligomers or even polymers. The simple ideas of electron delocalization in organic chemistry suggest that such polymers, if doped with electron or hole carriers, might be highly conductive. This indeed proves to be the case, and the resulting class of conductive polymers has been one of the most exciting and challenging new materials classes of the past two decades.[251-255]

The excitement really began when polyacetylene (CH)$_x$, doped with acceptors such as iodine, exhibited an increase of conductivity of nearly 10 orders of magnitude. Since then, a large number of related conductive polymers, including poly-thiophene, polypyrrole, poly-p-phenylene, and polyaniline, have been prepared and extensively studied.[251-255]

These materials are particularly challenging because of their polymeric nature: they do not form single crystals, and orientational defects, static disorder, and other materials imperfections are rife. Indeed, stretch drawing, to make the polymer strands more nearly parallel, increases the conductivity substantially.[256]

The critical notion for explaining conductivity in degenerate ground state polymers such as polyacetylene was actually suggested in a molecular context by Pople over 30 years ago.[257] The resonant structures shown in (XIII.1) are equally good representations of the ground state of nonatetraene. If the senses of conjugation change within the molecule, one can attain structure XIII.2. Note that the central carbon carries radical character, but no charge. Delocalization of this radical carrier along the chain should be relatively facile, but it is accompanied by a lattice distortion, corresponding roughly to the double bond characters shown in the valence bond structure of (XIII.2). This defect is called, currently, an uncharged soliton.[255] Closely related charged defects, referred to as polaron or bipolaron structures, are illustrated in (XIII.3) and (XIII.4). The existence of such structures has been demonstrated using both spectroscopy and computational techniques.[258,259] Charge transport in these materials occurs, apparently, not by simple band type conductivity as in a good metal, but rather by motion of soliton-like or polaron-like defects, a sort of intramolecular ET.

Contemporary Issues in Electron Transfer Research

J. Phys. Chem., Vol. 100, No. 31, 1996 **13165**

(a)

(b)   (XIII.1)

(XIII.2)

(XIII.3)

(XIII.4)
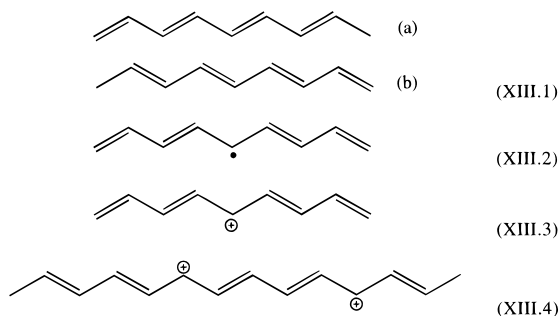
The conductivity properties of these materials can be truly impressive. As synthetic techniques permit more stereoregular, well-ordered polymeric chains to be prepared, the conductivities approach that of metallic copper. (In 1990, improved poly-acetylene exhibited a conductivity of 10^5 S/cm.[259])

These conductive polymers exhibit many of the characteristic properties of real metals. They show Pauli spin susceptibilities, thermopower linearly proportional to temperature, and heat capacities linearly proportional to temperature. All of these are characteristic of metals, with the Fermi level occurring in the midst of the continuous band of states. Improved materials have also exhibited metallic reflectivity (Drude edge in the infrared) and nonvanishing electronic conductivity at very low temperatures. None of the conductive polymers have yet been shown to exhibit the most obvious characteristic of a metal, decreasing conductivity with increasing temperature.

The explanation for this last phenomenon is one that should seem obvious: the limiting step for conductivity in extended systems is not transfer along a given conductive chain (extended like those in structure XIII.3), but rather transfer between chains. This bottle neck is responsible for the nonmetallic temperature dependence of the conductivity. Typical characteristic conductivity values perpendicular to the chain axis for highly oriented polyacetylenes are of the order of 100 S/cm, roughly comparable to Mott's minimum metallic conductivity criterion.[260] Tensile drawing can increase the mean free path and therefore the spatial extent of the localized states to several hundreds of lattice sites; nevertheless, interchain electron transfers are required for two- or three-dimensional conductivity.

It is perhaps striking that the conductive polymers apparently move charge by a mechanism quite different from that in superexchange-coupled electron donor acceptor materials: the electron is indeed localized along the chain and moves as a defect, rather than moving in an electronically coherent fashion without coupling to the vibrations. The exact relationship between conductive polymers and motion in extended donor/bridge/acceptor intramolecular electron transfer situations is yet to be completed, though some reports have appeared.[121,261−264] One certainly expects the temperature dependence to vary substantially between these two limits. (The temperature dependence may be dominated by reorganization energy considerations in superexchange coupled complexes and by conductivity temperature dependence in the more extended systems.)

The conductive polymer materials are of great intellectual challenge and possibly even greater commercial application. Many of the materials prepared so far are unstable and difficult to reproduce; nevertheless, the very broad bands, light weight, and chemical tailorability of these materials make them extremely attractive as advanced materials for, among other things, electrical interconnects and antistatic coatings.

XIV. Concluding Remarks

The intense and fruitful current research efforts in the area of electron transfer have led to broadly increased understanding of a large number of ET phenomena, rates, mechanisms, and reactivities. Our coverage has been selective. For example, we have not emphasized outer-sphere reactions and the Marcus cross-reaction equation. In other cases electron transfer is only part of the more complex mechanisms involved in such processes as corrosion, dissociative ET reactions, atom transfer, and proton-coupled electron transfer. They are illustrative of a number of very significant oxidation−reduction reactions where electron transfer plays a role, but there is an absence of understanding even at a semiquantitative level. These reactions are at the heart of many important catalytic and biological reactions. Much more needs to be learned about how they occur and about the microscopic details of the individual steps in which net electron transfer occurs.

Even among the situations in which we might expect the models and understandings that have been developed to hold pretty well, many aspects remain to be clearly interpreted. To cite only one example: The now quite old and standard data on the temperature dependence of the ET rate in *Chromatium vinosum* (Figure 7) were originally explained as arising from activated barrier crossing at high temperatures and nuclear tunneling (essentially temperature independent) at lower temperatures. While this is one possible explanation, a number of issues must be considered that cast doubt on this interpretation. First, the environment of the *C. vinosum* undergoes a glassy transition in this temperature range, and upon glassing, the solvent reorganization energy is modified by kinetic limitations.[29−31] Second, temperature can also effect the tunneling matrix element (breakdown of Condon approximation) and the dielectric constants. Therefore, a quantitative understanding of the temperature dependence is still lacking even for this standard system.[29−31,33,265]

The centrality of electron transfer phenomena in nature and in chemistry assures the ongoing vitality and richness of this field of research, which is, really, only now becoming a truly predictive and (in a few favorable cases) quantitative science. There is more day to dawn.[266]

References and Notes

(1) The most important usage of the words adiabatic and nonadiabatic involves the nature of the transfer process itself: Adiabatic electron transfers are envisioned as taking place on curves like those of Figure 2, in which the upper state is ignored; in this case, actual electronic coupling between minima decreases the barrier height, but does not effect the dynamic barrier top crossing. The nonadiabatic limit is one in which the splitting at the barrier top (the crossing point of Figure 5) is very small; essentially this is a condition on the magnitude of the H_{RP} matrix element. When this is true, one can use the golden rule as in eqs V.4. This limit is generally referred to as nonadiabatic electron transfer; the difference between adiabatic and nonadiabatic has to do with the relative magnitude of the H_{RP} matrix element compared to other energy quantities in the system such as the frequency, the inverse relaxation time, or the gap. Precise analysis of the relative adiabaticity or nonadiabaticity of ET reactions, the role of multidimensionality, and developing a general formalism that smoothly bridges adiabatic and nonadiabatic limits remain a major challenge in theoretical approaches to ET reactions.

(2) DeVault, D. *Quantum Mechanical Tunneling in Biological Systems*; Cambridge University Press: Cambridge, 1984.

(3) Ulstrup, J. *Charge Transfer Processes in Condensed Media, Lecture Notes in Chemistry*; Springer-Verlag: New York, 1979; Vol. 10.

(4) Newton, M. D.; Sutin, N. *Annu. Rev. Phys. Chem.* **1984**, *35*, 437.

(5) Newton, M. *Chem. Rev.* **1991**, *91*, 767.

(6) Marcus, R. A.; Sutin, N. *Biochim. Biophys. Acta* **1985**, *811*, 265.

(7) Mikkelsen, K. V.; Ratner, M. A. *Chem. Rev.* **1987**, *87*, 113.

(8) Kestner, N. R.; Logan, J.; Jortner, J. *J. Phys. Chem.* **1974**, *78*, 2148.

(9) Marcus, R. A. *Rev. Mod. Phys.* **1993**, *65*, 599.

(10) Schatz, G. C.; Ratner, M. A. *Quantum Mechanics in Chemistry*; Prentice-Hall: Englewood Cliffs: NJ, 1993; pp Chapter 10.

(11) Marcus, R. A. *J. Chem. Phys.* **1956**, *24*, 966.

(12) Marcus, R. A. *Annu. Rev. Phys. Chem.* **1964**, *15*, 155.

(13) Huang, J. K.; Warshel, A. *J. Am. Chem. Soc.* **1987**, *109*, 715.

(14) Taube, H. *Electron Transfer Reactions in Solution*; Academic: New York, 1970.

(15) Richardson, D. E.; Taube, H. *Coord. Chem. Rev.* **1984**, *60*, 107.

(16) Hush, N. S. *Trans. Faraday Soc.* **1961**, *57*, 557.

(17) Liu, Y.-P.; Newton, M. D. *J. Phys. Chem.* **1995**, *99*, 12382.

(18) Mikkelsen, K. V. *Z. Phys. Chem. (Munich)* **1991**, *170*, 8129.

(19) Kim, H. J.; Bianco, R.; Gertner, B. J.; Hynes, J. T. *J. Phys. Chem.* **1993**, *97*, 1723.

(20) Ferretti, A.; Lami, A.; Ondrechen, M. J.; Villani, G. *J. Phys. Chem.* **1995**, *99*, 10484.

(21) Schatz, P. N.; Piepho, S. B. *J. Phys. Chem.* **1994**, *98*, 11226.

(22) Neria, E.; Nitzan, A. *Chem. Phys.* **1994**, *183*, 351.

(23) Curtis, J. C.; Roberts, J. A.; Blackbourn, R. L.; Dong, Y.; Massum, M.; Johnson, C. S.; Hupp, J. T. *Inorg. Chem.* **1991**, *30*, 3856.

(24) Kuharski, R. A.; Bader, J. S.; Chandler, D.; Sprik, M.; Klein, M. L.; Impey, R. W. *J. Chem. Phys.* **1988**, *89*, 3248.

(25) Kneitel, C. L.; Newton, M. D.; Friedman, H. L. *J. Mol. Liq.* **1994**, *60*, 107.

(26) Sutin, N.; Brunschwig, B. S. *Adv. Chem. Ser.* **1990**, *226*, 64.

(27) Brunschwig, B. S.; Ehrenson, S.; Sutin, N. *J. Chem. Phys.* **1985**, *91*, 4714.

(28) Cammi, R.; Tomasi, J. *J. Chem. Phys.* **1994**, *100*, 7495.

(29) Gaines, G. L.; O'Neil, M. P.; Svec, W. A.; Niemczyk, M. P.; Wasielewski, M. R. *J. Am. Chem. Soc.* **1991**, *113*, 719.

(30) Hoffman, B. M.; Ratner, M. A. *Inorg. Chim. Acta* **1996**, *243*, 233.

(31) Agmon, N.; Rabinovich, S. *J. Chem. Phys.* **1992**, *97*, 7270.

(32) DeVault, D.; Chance, B. *Biophys. J.* **1966**, *6*, 825.

(33) Bixon, M.; Jortner, J. *J. Chem. Phys.* **1988**, *89*, 3392.

(34) Fischer, S. F.; Duyne, R. P. V. *Chem. Phys.* **1977**, *26*, 9.

(35) Jortner, J. *J. Chem. Phys.* **1976**, *64*, 4860.

(36) Van Duyne, R. P.; Fischer, S. F. *Chem. Phys.* **1976**, *5*, 183.

(37) Schmidt, P. P. *Electrochem. Spec. Period. Rep.* **1978**, *6*, 128.

(38) Hopfield, J. J. *PNAS* **1974**, *71*, 3640.

(39) Scher, H.; Holstein, T. *Philos. Mag. B* **1981**, *44*, 343.

(40) Holstein, T. *Ann. Phys.* **1959**, *8*, 343.

(41) Kubo, R.; Toyozawa, Y. *Prog. Theor. Phys.* **1955**, *13*, 60.

(42) Jortner, J.; Bixon, M. *Ber. Bunsen-Ges. Phys. Chem.* **1995**, *99*, 296.

(43) Zusman, L. D. *Chem. Phys.* **1980**, *49*, 295.

(44) Nadler, W.; Marcus, R. A. *J. Chem. Phys.* **1987**, *86*, 3906.

(45) Bixon, M.; Jortner, J. *Chem. Phys.* **1993**, *176*, 476.

(46) Fonseca, T.; Kim, H. J.; Hynes, J. T. *J. Mol. Liq.* **1994**, *60*, 161.

(47) Weaver, M. J. *J. Mol. Liq.* **1994**, *60*, 57.

(48) Nagasawa, Y.; Yartsev, A. P.; Tominaga, K.; Bisht, P. B.; Johnson, A. E.; Yoshihara, K. *J. Phys. Chem.* **1995**, *99*, 653.

(49) Barbara, P. F.; Jarzeba, W. *Adv. Photochem.* **1990**, *15*, 1.

(50) Barbara, P. F.; Walker, G. C.; Smith, T. P. *Science (Washington, D.C.)* **1992**, *256*, 975.

(51) Johnson, A. E.; Levinger, N. E.; Jarzeba, W.; Schlief, R. E.; Kliner, D. A. V.; Barbara, P. F. *Chem. Phys.* **1993**, *176*, 555.

(52) Reid, P. J.; Silva, C.; Barbara, P. F.; Karki, L.; Hupp, J. T. *J. Phys. Chem.* **1995**, *99*, 2609.

(53) Reid, P. J.; Barbara, P. F. *J. Phys. Chem.* **1995**, *99*, 3554.

(54) Hoffman, B. M.; Ratner, M. A. *J. Am. Chem. Soc.* **1987**, *109*, 6257.

(55) Brunschwig, B. S.; Sutin, N. *J. Am. Chem. Soc.* **1989**, *111*, 7456.

(56) Bechtold, R.; Kuehn, C.; Lepre, C.; Isied, S. S. *Nature* **1986**, *322*, 286.

(57) Libby, W. F. *J. Phys. Chem.* **1952**, *56*, 86.

(58) Cao, J.; Minichino, C.; Voth, G. A. *J. Chem. Phys.* **1995**, *103*, 1391.

(59) Egger, R.; Mak, C. H.; Weiss, U. *J. Chem. Phys.* **1994**, *100*, 2651.

(60) Makarov, D.; Makri, N. *Chem. Phys. Lett.* **1994**, *221*, 482.

(61) Song, X.; Stuchebrukhov, A. A. *J. Chem. Phys.* **1993**, *99*, 969.

(62) Guo, H.; Liu, L.; Lao, K. *Chem. Phys. Lett.* **1994**, *218*, 212.

(63) Hammerich, A.; Nitzan, A.; Ratner, M. A. *Theor. Chim. Acta* **1994**, *89*, 383.

(64) Evans, D.; Nitzan, A. To be published.

(65) Klimkans, A.; Larsson, S. *Chem. Phys.* **1994**, *189*, 25.

(66) Basilevsky, M. V.; Chudinov, G. E. *J. Chem. Phys.* **1995**, *103*, 1470.

(67) Leggett, A. J.; Chakravarty, S.; Dorsey, A. T.; Fisher, M. P. A.; Garg, A.; Zwerger, W. *Rev. Mod. Phys.* **1987**, *59*, 1.

(68) Tanimura, Y.; Wolynes, P. G. *J. Chem. Phys.* **1992**, *96*, 8485.

(69) Bixon, M.; Jortner, J.; Cortes, J.; Heitele, H.; Michel-Beyerle, M. E. *J. Phys. Chem.* **1994**, *98*, 7289.

(70) Wiederrecht, G. P.; Niemczyk, M. P.; Svec, W. A.; Wasielewski, M. R. *J. Am. Chem. Soc.* **1996**, *118*, 81.

(71) Spears, K. G.; Wen, X.; Zhang, R. *J. Phys. Chem.* **1996**, *100*, 10206.

(72) Doorn, S. K.; Stoutland, P. O.; Dyer, R. B.; Woodruff, W. H. *J. Am. Chem. Soc.* **1992**, *114*, 3133.

(73) Spears, K. G.; Wen, X.; Arrivo, S. M. *J. Phys. Chem.* **1994**, *98*, 9693.

(74) Walker, G. C.; Barbara, P. F.; Doorn, S. K.; Yuhua, D.; Hupp, J. T. *J. Phys. Chem.* **1991**, *95*, 5712.

(75) Doorn, S. K.; Blackbourn, R. L.; Johnson, C. S.; Hupp, J. T. *Electrochim. Acta* **1991**, *36*, 1775.

(76) Kulinowski, K.; Gould, I. R.; Myers, A. B. *J. Phys. Chem.* **1995**, *99*, 9017.

(77) Shin, K. S.; Zink, J. I. *J. Am. Chem. Soc.* **1990**, *112*, 7148.

(78) Trulson, M. O.; Dollinger, G. D.; Mathies, R. A. *J. Am. Chem. Soc.* **1987**, *109*, 586.

(79) Closs, G. L.; Miller, J. R. *Science (Washington, D.C.)* **1988**, *240*, 440.

(80) Mikkelsen, K. V.; Pedersen, S. U.; Lund, H.; Swanstrom, P. *J. Phys. Chem.* **1991**, *95*, 8892.

(81) Sutin, N. *Prog. Inorg. Chem.* **1983**, *30*, 441.

(82) Abruna, H. D.; White, J. H.; Albarelli, G.; Bommarito, M.; Bedzyk, M. J.; McMillan, M. *J. Phys. Chem.* **1988**, *97*, 7045.

(83) Tannor, D. J.; Heller, E. J. *J. Chem. Phys.* **1982**, *77*, 202.

(84) Coalson, R. D.; Evans, D. G.; Nitzan, A. *J. Chem. Phys.* **1994**, *101*, 436.

(85) Spears, K. G. *J. Phys. Chem.* **1995**, *99*, 2469.

(86) Todd, M. D.; Nitzan, A.; Ratner, M. A.; Hupp, J. T. *J. Photochem. Photobiol. A* **1994**, *82*, 87.

(87) Marcus, R. A. *Discuss. Faraday Soc.* **1960**, *29*, 21.

(88) Marcus, R. A. *Angew. Chem., Int. Ed. Engl.* **1993**, *32*, 1111.

(89) Meyer, T. J. *Acc. Chem. Res.* **1989**, *22*, 1048.

(90) Mirkin, C. A.; Ratner, M. A. *Annu. Rev. Phys. Chem.* **1992**, *43*, 719.

(91) Gust, D.; Moore, T. A.; Moore, A. M. *Acc. Chem. Res.* **1993**, *26*, 198.

(92) Wasielewski, M. R. *Chem. Rev.* **1992**, *92*, 435.

(93) Gust, D.; Moore, T. A.; Moore, A. L.; Macpherson, A. N.; Lopez, A.; DeGraziano, J. M.; Gouni, I.; Bittersman, E.; Seely, G. R.; Gao, F.; Nieman, R. A.; Ma, X. C.; Demanche, L. J.; Hung, S.-C.; Luttrull, D. K.; Lee, S.-J.; Kerrigan, P. K. *J. Am. Chem. Soc.* **1993**, *115*, 11141.

(94) Wasielewski, M. R.; Gaines III, G. L.; Wiederrecht, G. P.; Svec, W. A.; Niemczyk, M. P. *J. Am. Chem. Soc.* **1993**, *115*, 10442.

(95) Gunderman, K.-D.; McCapra, F. *Chemiluminescence in Organic Chemistry*; Springer-Verlag: New York, 1987; p 145.

(96) Collinson, M. M.; Pastore, P.; Wightman, R. M. *J. Phys. Chem.* **1994**, *98*, 11942.

(97) Miller, J. R.; Calcaterra, L. T.; Closs, G. L. *J. Am. Chem. Soc.* **1984**, *97*, 3047.

(98) McLendon, G.; Miller, J. R. *J. Am. Chem. Soc.* **1989**, *107*, 7781.

(99) Siebrand, W. *J. Chem. Phys.* **1971**, *55*, 5843.

(100) Freed, K. F. *Top. Curr. Chem.* **1972**, *31*, 65.

(101) Freed, K. F.; Jortner, J. *J. Chem. Phys.* **1970**, *62*, 72.

(102) Englman, R.; Jortner, J. *Mol. Phys.* **1970**, *18*, 145.

(103) Chen, P.; Duesing, R.; Graff, D. K.; Meyer, T. J. *J. Phys. Chem.* **1991**, *95*, 5850.

(104) Chen, P.; Mecklenburg, S. L.; Duesing, R.; Meyer, T. J. *J. Phys. Chem.* **1993**, *97*, 6811.

(105) Gould, I. R.; Noukakis, D.; Gomez-Jahn, L.; Young, R. H.; Goodman, J. L.; Farid, S. *Chem. Phys.* **1993**, *176*, 439.

(106) Gould, I. R.; Ege, D.; Mattes, S. L.; Farid, S. *J. Am. Chem. Soc.* **1987**, *109*, 3794.

(107) Wuttke, D. S.; Bjerrum, M. J.; Chang, I.-J.; Winkler, J. R.; Gray, H. B. *Biochim. Biophys. Acta* **1992**, *1101*, 168.

(108) Onuchic, J. N.; Beratan, D. N.; Winkler, J. R.; Gray, H. B. *Annu. Rev. Phys. Chem.* **1992**, *21*, 349.

(109) Peterson-Kennedy, S. E.; McGourty, J. L.; Kalweit, J. A.; Hoffman, B. M. *J. Am. Chem. Soc.* **1986**, *108*,

(110) Axup, A. W.; Albin, M.; Mayo, S. L.; Crutchley, R. J.; Gray, H. G. *J. Am. Chem. Soc.* **1988**, *110*, 435.

(111) Heitele, H.; Michel-Beyerle, M. E. In *Antennas and Reaction Centers of Photosynthetic Bacteria*; Michel-Beyerle, M. E., Ed.; Springer-Verlag: Berlin, 1985.

(112) Paddon-Row, M. N.; Verhoeven, J. W. *New J. Chem.* **1991**, *15*, 107.

(113) Joran, A. D.; Leland, B. A.; Felker, P. M.; Zewail, A. H.; Hopfield, J. J.; Dervan, P. B. *Nature* **1987**, *327*, 508.

(114) Ratner, M. A. *J. Phys. Chem.* **1990**, *94*, 4877.

(115) McConnell, H. M. *J. Chem. Phys.* **1961**, *35*, 508.

(116) Hoffman, R. *Acc. Chem. Res.* **1971**, *4*, 1.

(117) Larsson, S. *J. Chem. Soc., Faraday Trans.* **1981**, *79*, 1575.

(118) Larsson, S.; Volosov, A. *J. Chem. Phys.* **1987**, *87*, 6623.

(119) Curtiss, L. A.; Naleway, C. A.; Miller, J. R. *Chem. Phys.* **1993**, *176*, 387.

(120) Sheppard, M. S.; Paddon-Row, M. N.; Jordan, K. D. *Chem. Phys.* **1993**, *176*, 289.

(121) Felts, A. K.; Pollard, W. T.; Friesner, R. A. *J. Phys. Chem.* **1995**, *99*, 2929.

(122) Skourtis, S. S.; Beratan, D. N.; Onuchic, J. *Chem. Phys.* **1993**, *176*, 501.

(123) Scherer, P. O. J.; Fischer, S. F. *J. Phys. Chem.* **1989**, *93*, 1633.

(124) Reimers, J. R.; Hush, N. S. *J. Photochem. Photobiol.* **1994**, *82*, 31.

Contemporary Issues in Electron Transfer Research

J. Phys. Chem., Vol. 100, No. 31, 1996 **13167**

(125) Moser, C. C.; Keske, J. M.; Warncke, K.; Farid, R. S.; Dutton, P. L. *Nature* **1992**, *355*, 796.

(126) Newton, M. D.; Cave, R. In *Molecular Electronics*; Ratner, M. A., Jortner, J., Eds.; IUPAC: London, 1996.

(127) Ogawa, M. Y.; Wishart, J. F.; Young, Z.; Miller, J. R.; Isied, S. S. *J. Phys. Chem.* **1993**, *97*, 11456.

(128) Barton, J. K.; Kumar, C. V.; Turro, N. J. *J. Am. Chem. Soc.* **1986**, *108*, 6391.

(129) Arkin, M. R.; Stemp, E. D. A.; Jenkins, Y.; Barbara, P. F.; Turro, N. J.; Barton, J. K. *Polym. Mater. Sci. Eng.* **1994**, *71*, 598.

(130) Arkin, M. R.; Jenkins, Y.; Murphy, C. J.; Turro, N. J.; Barton, J. K. *Adv. Chem. Ser.*, in press.

(131) Robin, M. B.; Day, P. *Adv. Inorg. Chem. Radiochem.* **1967**, *10*,

(132) Allen, G. C.; Hush, N. S. *Prog. Inorg. Chem.* **1967**, *8*, 357.

(133) Hush, N. S. *Prog. Inorg. Chem.* **1967**, *8*, 391.

(134) Hush, N. S. *Coord. Chem. Rev.* **1985**, *64*, 135.

(135) Creutz, C. *Prog. Inorg. Chem.* **1983**, *30*, 1.

(136) Creutz, C.; Taube, H. *J. Am. Chem. Soc.* **1973**, *95*, 1086.

(137) Oh, D. H.; Sano, M.; Boxer, S. G. *J. Am. Chem. Soc.* **1991**, *113*, 6880.

(138) Hupp, J. T.; Neyhart, G.; Meyer, T. J.; Kober, E. K. *J. Phys. Chem.* **1992**, *96*, 10820.

(139) Powers, M. J.; Meyer, T. J. *J. Am. Chem. Soc.* **1978**, *100*, 4393.

(140) Brunschwig, B. S.; Ehrenson, S.; Sutin, N. *J. Phys. Chem.* **1986**, *90*, 3657.

(141) Kober, E. M.; Goldsby, K. A.; Narayana, D. N. S.; Meyer, T. J. *J. Am. Chem. Soc.* **1983**, *105*,

(142) Curtis, J. C.; Sullivan, B. P.; Meyer, T. J. *Inorg. Chem.* **1983**, *22*, 224.

(143) Blackbourn, R. L.; Hupp, J. T. *J. Phys. Chem.* **1988**, *92*, 2817.

(144) Hupp, J. T.; Neyhart, G. A.; Meyer, T. J. *J. Am. Chem. Soc.* **1986**, *108*, 5349.

(145) Hupp, J. T.; Neyhart, G. A.; Meyer, T. J., in press.

(146) Nelsen, S. F.; Adamus, J.; Wolff, J. *J. Am. Chem. Soc.* **1994**, *116*, 1589.

(147) Dubicki, L.; Ferguson, J.; Krausz, E. R. *J. Am. Chem. Soc.* **1985**, *107*, 179.

(148) Zhang, L.-T.; Ko, J.; Ondrechen, M. J. *J. Phys. Chem.* **1989**, *93*, 3030.

(149) Piepho, S. B.; Krausz, E. R.; Schatz, P. N. *J. Am. Chem. Soc.* **1978**, *100*, 6319.

(150) Piepho, S. B. *J. Am. Chem. Soc.* **1990**, *112*, 4197.

(151) Steinfeld, J. I. *Molecules and Radiation*; The MIT Press: Cambridge, 1985.

(152) Jortner, J. *Philos. Mag.* **1979**, *B40*, 317.

(153) Sutin, N. *Adv. Chem. Ser.* **1991**, *228*, 25.

(154) Su, S. G.; Simon, J. D. *J. Chem. Phys.* **1988**, *89*, 908.

(155) Rettig, W. *J. Phys. Chem.* **1982**, *86*, 1970.

(156) Katz, N. E.; Mecklenburg, S. L.; Graff, D. K.; Chen, P.; Meyer, T. J. *J. Phys. Chem.* **1994**, *98*, 8959.

(157) Kober, E. M.; Caspar, J. V.; Lumpkin, R. S.; Meyer, T. J. *J. Phys. Chem.* **1986**, *90*, 3722.

(158) Yoshihara, K.; Tominaga, K.; Nagasawa, Y. *Bull. Chem. Soc. Jpn.* **1995**, *68*, 696.

(159) Heitele, H. *Angew. Chem., Int. Ed. Engl.* **1993**, *32*, 359.

(160) Wiederrecht, G. P.; Svec, W. A.; Niemczyk, M. P.; Wasielewski, M. R. *J. Phys. Chem.* **1995**, *99*, 8918.

(161) Rossky, P. J.; Simon, J. D. *Nature* **1994**, *370*, 263.

(162) Wynne, K.; Galli, C.; Hochstrasser, R. M. *J. Chem. Phys.* **1994**, *100*, 4797.

(163) Vilarreal, P.; Miret-Artes, S.; Roncero, O.; Delgado-Bario, G.; Beswick, J. A.; Halberstadt, N.; Coalson, R. D. *J. Chem. Phys.* **1991**, *94*, 4230.

(164) Mataga, N.; Nishikawa, S.; Asahi, T.; Okada, T. *J. Phys. Chem.* **1990**, *94*, 1443.

(165) Miyasaka, H.; Tabata, A.; Kamada, K.; Mataga, N. *J. Am. Chem. Soc.* **1993**, *115*, 7335.

(166) Asahi, T.; Mataga, N. *J. Phys. Chem.* **1991**, *95*, 1956.

(167) Hynes, J. T. *Understanding Chem. React.* **1994**, *7*, 345.

(168) Smith, B. B.; Staib, A.; Hynes, J. T. *Chem. Phys.* **1993**, *176*, 521.

(169) Hynes, J. T. *J. Phys. Chem.* **1986**, *90*, 3701.

(170) Maroncelli, M.; MacInnis, J.; Fleming, G. *Science (Washington, D.C.)* **1989**, *243*, 1674.

(171) Fleming, G. R.; VanGrondelle, R. *Phys. Today* **1994**, *47*, 48.

(172) Franzen, S. F.; Martin, J.-L. *Annu. Rev. Phys. Chem.* **1995**, *46*, 453.

(173) Michel-Beyerle, M. E.; Small, G. J.; Hochstrasser, R. M.; Hofacker, G. L. *Chem. Phys.* **1995**, *197*, 223 (special issue).

(174) Murphy, C. J.; Arkin, M. R.; Jenkins, Y.; Ghatlia, N. D.; Bossmann, S.; Turro, N. J.; Barton, J. K. *Science* **1993**, *262*, 1025.

(175) Stemp, E. D. A.; Arkin, M. R.; Barton, J. K. *J. Am. Chem. Soc.* **1995**, *117*, 2375.

(176) Simon, J. D.; Doolen, R. *J. Am. Chem. Soc.* **1992**, *114*, 4861.

(177) Simon, J. D.; Su, S.-G. *J. Chem. Phys.* **1987**, *87*, 7016.

(178) O'Driscoll, E.; Simon, J. D.; Peters, K. S. *J. Am. Chem. Soc.* **1990**, *112*, 7091.

(179) Thompson, P. A.; Simon, J. D. *J. Am. Chem. Soc.* **1993**, *115*, 5657.

(180) Tominaga, K.; Kliner, D. A. V.; Johnson, A. E.; Levinger, N. E.; Barbara, P. F. *J. Chem. Phys.* **1993**, *98*, 1228.

(181) Reid, P. J.; Alex, S.; Jarzeba, W.; Schlief, R. E.; Johnson, A. E.; Barbara, P. F. *Chem. Phys. Lett.* **1994**, *229*, 93.

(182) Poellinger, F.; Heitele, H.; Michel-Beyerle, M. E.; Anders, C.; Futscher, M.; Staab, H. A. *Chem. Phys. Lett.* **1992**, *198*, 645.

(183) Doorn, S. K.; Dyer, R. B.; Stoutland, P. O.; Woodruff, W. H. *J. Am. Chem. Soc.* **1993**, *115*, 6398.

(184) Jarzeba, W.; Schlief, R. E.; Barbara, P. F. *J. Phys. Chem.* **1994**, *98*, 9102.

(185) Schlief, R. E.; Jarzeba, W.; Thakur, K. A. M.; Alfano, J. C.; Barbara, P. F. *J. Mol. Liq.* **1994**, *60*, 201.

(186) Hörmann, A.; Jarzeba, W.; Barbara, P. F. *J. Phys. Chem.* **1995**, *99*, 2006.

(187) Dakhnovskii, Y. I.; Doolen, R.; Simon, J. D. *J. Chem. Phys.* **1994**, *101*, 6640.

(188) Doolen, R.; Simon, J. D. *J. Am. Chem. Soc.* **1994**, *116*, 1155.

(189) Heitele, H. Submitted, 1994.

(190) Calef, D. F.; Wolynes, P. G. *J. Phys. Chem.* **1983**, *87*, 3387.

(191) Sumi, H.; Marcus, R. A. *J. Chem. Phys.* **1986**, *84*, 4894.

(192) Yan, Y. J.; Sparpaglione, M.; Mukamel, S. *J. Phys. Chem.* **1988**, *92*, 4842.

(193) Rips, I.; Jortner, J. *J. Chem. Phys.* **1987**, *87*, 2090.

(194) Bagchi, B.; Fleming, G. R. *J. Phys. Chem.* **1990**, *94*, 9.

(195) Zhu, J.; Rasaiah, J. C. *J. Chem. Phys.* **1991**, *95*, 3325.

(196) Rasaiah, J. C.; Zhu, J. *J. Chem. Phys.* **1993**, *98*, 1213.

(197) Mukamel, S.; Bosma, W. In *Proceedings of the 29th Yamada Conference*; North-Holland: Amsterdam, 1991; p 195.

(198) Tully, J. C.; Preston, R. K. *J. Chem. Phys.* **1971**, *55*, 562.

(199) Tully, J. C. *J. Chem. Phys.* **1990**, *93*, 1061.

(200) Webster, F. J.; Schnitker, J.; Friedrichs, M. S.; Friesner, R. A.; Rossky, P. J. *Phys. Rev. Lett.* **1991**, *66*, 3172.

(201) Webster, F.; Rossky, P. J.; Friesner, R. A. *Comput. Phys. Commun.* **1991**, *63*, 494.

(202) Neria, E.; Nitzan, A.; Barnett, R. N.; Landman, U. *Phys. Rev. Lett.* **1991**, *67*, 1011.

(203) Neria, E.; Nitzan, A. *J. Chem. Phys.* **1993**, *99*, 1109.

(204) Chandler, D.; Wolynes, P. G. *J. Chem. Phys.* **1981**, *74*, 4078.

(205) Thirumalai, D.; Berne, B. J. *Comput. Phys. Commun.* **1991**, *63*, 415.

(206) Makri, N. *Comput. Phys. Commun.* **1991**, *63*, 389.

(207) Berne, B. J.; Thirumalai, D. *Annu. Rev. Phys. Chem.* **1986**, *37*, 401.

(208) Parrinello, M.; Rahman, A. *J. Chem. Phys.* **1984**, *80*, 860.

(209) Landman, U.; Scharf, D.; Jortner, J. *Phys. Rev. Lett.* **1985**, *54*, 1860.

(210) Jean, J. M.; Fleming, G. R. *J. Chem. Phys.* **1995**, *103*, 2092.

(211) Coker, D. F.; Xiao, L. J. *J. Chem. Phys.* **1995**, *102*, 4695.

(212) Jimenez, R.; Fleming, G. R.; Kumar, P. V.; Maroncelli, M. *Nature* **1994**, *369*, 471.

(213) Maroncelli, M. *J. Mol. Liq.* **1993**, *57*, 1.

(214) Friedman, H. L.; Raineri, F. O.; Hirata, F.; Perng, B. C. *J. Stat. Phys.* **1995**, *78*, 239.

(215) Cho, M.; Fleming, G. R.; Saito, S.; Ohmine, I.; Stratt, R. M. *J. Chem. Phys.* **1994**, *100*, 6672.

(216) Bagchi, B. *Annu. Rev. Phys. Chem.* **1989**, *40*, 115.

(217) Raineri, F. O.; Resat, H.; Perng, B.-C.; Hirata, F.; Friedman, H. L. *J. Chem. Phys.* **1994**, *100*, 1477.

(218) Schwartz, B. J.; Rossky, P. J. *J. Phys. Chem.* **1995**, *99*, 2953.

(219) Carter, E. A.; Hynes, J. T. *J. Chem. Phys.* **1991**, *94*, 5961.

(220) Bader, J. S.; Chandler, D. *Chem. Phys. Lett.* **1989**, *157*, 501.

(221) Ladanyi, B. M.; Stratt, R. M. *J. Phys. Chem.* **1995**, *99*, 2502.

(222) Stratt, R. M. *Acc. Chem. Res.* **1995**, *28*, 201.

(223) Kang, T. J.; Kahlow, M. A.; Giser, D.; Swallen, S.; Nagarajan, V.; Jarzeba, W.; Barbara, P. F. *J. Phys. Chem.* **1988**, *92*, 6800.

(224) Kang, T. J.; Jarzeba, W.; Barbara, P. F.; Fonseca, T. *Chem. Phys.* **1990**, *149*, 81.

(225) Tominaga, K.; Walker, G. C.; Kang, T. J.; Barbara, P. F. *J. Phys. Chem.* **1991**, *95*, 10485.

(226) Doorn, S. K.; Hupp, J. T. *J. Am. Chem. Soc.* **1989**, *111*, 1142.

(227) Vos, M. H.; Rappaport, F.; Lambry, J.-C.; Breton, J.; Martin, J.-L. *Nature* **1993**, *363*, 320.

(228) Vos, M. H.; Jones, M. R.; Hunter, C. N.; Breton, J.; Lambry, J.-C.; Martin, J.-L. *Biochemistry* **1994**, *33*, 6750.

(229) Bradforth, S. E.; Jimenez, R.; Mourik, F. v.; Grondelle, R. v.; Fleming, G. R. *J. Phys. Chem.* **1995**, *99*, 16179.

(230) Arnett, D. C.; Vöhringer, P.; Scherer, N. F. *J. Am. Chem. Soc.* **1995**, *117*, 12262.

(231) Wang, Q.; Schoenlein, R. W.; Peteanu, L. A.; Mathies, R. A.; Shank, C. V. *Science (Washington, D.C.)* **1994**, *266*, 422.

(232) Schoenlein, R. W.; Peteanu, L. A.; Mathies, R. A.; Shank, C. V. *Science (Washington, D.C.)* **1992**, *254*, 412.

(233) Jortner, J.; Bixon, M. *J. Chem. Phys.* **1988**, *88*, 167.

(234) Roy, S.; Bagchi, B. *J. Chem. Phys.* **1995**, *102*, 7937.

(235) Roy, S.; Bagchi, B. *J. Chem. Phys.* **1994**, *100*, 8802.

(236) Johnson, A. J.; Levinger, N. E.; Jarzeba, W.; Schlief, R. E.; Kliner, D. A. V.; Barbara, P. F. *Chem. Phys.* **1993**, *176*, 555.

(237) Walker, G. C.; Åkesson, E.; Johnson, A. E.; Levinger, N. E.; Barbara, P. F. *J. Phys. Chem.* **1992**, *96*, 3728.

(238) Johnson, A. E.; Levinger, N. E.; Walker, G. C.; Barbara, P. F. *Ultrafast Phenom. VIII* **1993**.

(239) Schlag, E. W.; Schneider, S.; Fischer, S. F. *Annu. Rev. Phys. Chem.* **1971**, *22*, 465.

(240) Henry, B. R.; Siebrand, W. In *Organic Molecular Photophysics*; Birks, J. B., Ed.; Wiley: New York, 1973; p 153.

(241) Hammes-Schiffer; Tully, J. C. *J. Chem. Phys.* **1995**, *103*, 8525.

(242) Berendsen, H. J. C.; Mavri, J. *Int. J. Quantum Chem.* **1996**, *57*, 975.

(243) Jortner, J.; Bixon, M.; Wegewijs, B.; Verhoeven, J. W.; Rettschnick, R. H. P. *Chem. Phys. Lett.* **1993**, *205*, 451.

(244) Wegewijs, B.; Ng, A. K. F.; Rettschnick, R. H. P.; Verhoeven, J. W. *Chem. Phys. Lett.* **1992**, *200*, 357.

(245) Felker, P. M.; Syage, J. A.; Lambert, W. R.; Zewail, A. H. *Chem. Phys. Lett.* **1982**, *92*, 1.

(246) Bixon, M.; Jortner, J.; Verhoeven, J. W. *J. Am. Chem. Soc.* **1994**, *116*, 7349.

(247) Richardson, D. E.; Eyler, J. R. *Chem. Phys.* **1993**, *176*, 457.

(248) In fact, forming the folded (harpooned) charge transfer exciplex from the initially formed, extended D^+BA^- is more complex. The actual kinetic scheme corresponds to the energy level diagram schematically indicated in Figure 15. Two rate constants, k_{ET} and k_{FOLD}, correspond in the first case to transfer from the initially excited (DBA)* species to the extended D^+BA^- species; following this, harpooning occurs, driven by strongly anharmonic couplings, to provide the (bent, folded, harpooned, docked) structure, which then undergoes charge transfer emission.

(249) Rehm, D.; Weller, A. *Isr. J. Chem.* **1970**, *8*, 259.

(250) Magee, J. *J. Chem. Phys.* **1940**, *8*, 687.

(251) Menon, R.; Yoon, C. O.; Moses, D.; Heeger, A. J., in press.

(252) *Handbook of Conducting Polymers*; Skotheim, T. A., Ed.; M. Dekker: New York, 1986.

(253) *Conjugated Polymers and Related Materials: The Interconnection of Chemical and Electronic Structure: Proceedings of the Eighty-First Nobel Symposium*; Salaneck, W. R.; Lunstrom, I.; Ranby, B., Eds.; Oxford University Press: New York, 1993.

(254) *Intrinsically Conducting Polymers: An Emerging Technology*; Aldissi, M., Ed.; Kluwer Academic: Dordrecht, 1993.

(255) *Solitons and Polarons in Conducting Polymers*; Lu, Y., Ed.; World Scientific: Singapore, 1988.

(256) Reghu, M.; Vakipatta, K.; Yoon, C. O.; Cao, Y.; Moses, D. *Synth. Met.* **1994**, *65*, 167.

(257) Pople, J. A.; Walmsley, S. H. *Mol. Phys.* **1962**, *5*, 15.

(258) Loegdlund, M.; Bredas, J. L. *J. Chem. Phys.* **1995**, *103*, 4201.

(259) Tsukamoto, J. *Adv. Phys.* **1992**, *41*, 509.

(260) Mott, N. F. *Metal-Insulator Transitions;* 2nd ed.; Taylor & Francis: London, 1990.

(261) Hey, R.; Schreiber, M. *J. Chem. Phys.* **1995**, *103*, 10726.

(262) Wasielewski, M. R.; Johnson, D. C.; Svec, W. A.; Kersey, R. M.; Cragg, D. S.; Minsek, D. W. In *Photochemical Energy Conversion*; Norris, J. R., Meisel, D., Eds.; Elsevier: Amsterdam, 1985; p 135.

(263) Janssen, R. A. J.; Christiaans, M. P. T.; Hare, C.; Martin, N.; Sariciftci, N. S.; Heeger, A. J.; Wuld, F. *J. Chem. Phys.* **1995**, *103*, 8840.

(264) Cornil, J.; Beljonne, D.; Bredas, J. L. *J. Chem. Phys.* **1995**, *103*, 842.

(265) Lubchenko, V.; Wolynes, P. G. *J. Chem. Phys.* **1996**, *104*, 1875.

(266) Thoreau, H. D. *Walden*; Clarkson N. Potter: 1970.